Eur. Phys. J. C (2015) 75:261
DOI 10.1140/epjc/s10052-015-3486-6

THE EUROPEAN PHYSICAL JOURNAL C

Regular Article - Theoretical Physics

Generalized parton distributions and transverse densities in a light-front quark–diquark model for the nucleons

Chandan Mondal, Dipankar Chakrabarti[a]

Department of Physics, Indian Institute of Technology Kanpur, Kanpur 208016, India

Received: 23 February 2015 / Accepted: 27 May 2015 / Published online: 12 June 2015

Abstract We present a study of the generalized parton distributions (GPDs) for the quarks in a proton in both momentum and position spaces using the light-front wave functions (LFWFs) of a quark–diquark model for the nucleon predicted by the soft-wall model of AdS/QCD. The results are compared with the soft-wall AdS/QCD model of proton GPDs for zero skewness. We also calculate the GPDs for nonzero skewness. We observe that the GPDs have a diffraction pattern in longitudinal position space, as seen before in other models. Then we present a comparative study of the nucleon charge and anomalous magnetization densities in the transverse plane. Flavor decompositions of the form factors and transverse densities are also discussed.

1 Introduction

Hadronic structure and their properties being nonperturbative in nature are always very difficult to evaluate from QCD first principles and there have been numerous attempts to gain insight into hadrons by studying QCD inspired models. The quark–diquark model, where a nucleon is considered to be a bound state of a single quark and a scalar or vector diquark state, is proven to reproduce many interesting properties of the nucleons and has been extensively used to investigate the proton structure. Recently, a light-front quark–diquark model for the nucleons has been proposed in Ref. [1], where the light-front wave functions are modeled by the wave functions obtained from a soft-wall model in light-front AdS/QCD. The light-front wave functions (LFWFs) are derived by matching the electromagnetic form factors of hadrons in the light front QCD and soft-wall model of AdS/QCD. The model is consistent with the Drell–Yan–West relation relating the high Q^2 behavior of the nucleon form factors and the large x behavior of the structure functions. Recently, LFWFs of baryon and the light baryon spectrum have been described by extending the superconformal quantum mechanics to the light front and embedding it in AdS space [2]. The LFWF for the rho meson in AdS/QCD has been successfully applied to predict the diffractive rho meson electroproduction [3].

In this paper, we study the proton structure and evaluate the Generalized Parton Distributions (GPDs), transverse charge and magnetization densities in the light-front quark–diquark model. Contrary to ordinary parton distribution functions, GPDs are functions of three variables, namely, longitudinal momentum faction x of the quark or gluon, the square of the total momentum transferred (t) and the skewness ζ, which represents the longitudinal momentum transferred in the process, and they provide interesting information about the spin and orbital angular momentum of the constituents, as well as the spatial structure, of the nucleons (see [4–6] for reviews on GPDs). The GPDs appear in the exclusive processes like deeply virtual Compton scattering (DVCS) or vector meson productions and they reduce to the ordinary parton distributions in the forward limit. Their first moments are related to the form factors and the second moments of the sum of the GPDs are related to the angular momentum by a sum rule proposed by Ji [7]. Being off-forward matrix elements, the GPDs have no probabilistic interpretation. But for zero skewness, the Fourier transforms of the GPDs with respect to the transverse momentum transfer ($\Delta_\perp$) give the impact parameter dependent GPDs which satisfy the positivity condition and can be interpreted as distribution functions [8]. The transverse impact parameter dependent GPDs provide us with the information about partonic distributions in the impact parameter or the transverse position space for a given longitudinal momentum (x). The impact parameter $b_\perp$ gives the separation of the struck quark from the center of momentum. In parallel to the efforts to understand the GPDs by theoretical modeling, different experiments are also measuring deeply virtual Compton scattering and deeply virtual meson production to gain insight and experimentally constrain the GPDs [9–13].

[a] e-mail: dipankar@iitk.ac.in

We evaluate the proton GPDs for both zero and nonzero skewness and compared with the results in a soft-wall AdS/QCD model [14] (for hard-wall and soft-wall AdS/QCD models of hadrons, see [15–20]). For zero skewness, the GPDs are investigated in the impact parameter or transverse position space. The LF diquark results for the GPD $H(x, b_\perp)$ for the u-quark is almost the same as AdS/QCD results whereas there is a little difference for the d-quark. But the LF diquark model results for $E(x, b_\perp)$ for both u- and d-quarks are different from the AdS/QCD results. For nonzero skewness, the GPDs in longitudinal impact parameter space show a diffraction pattern. It is interesting to note that similar diffraction patterns were observed in a simple QED model for the DVCS amplitude [21,22] and GPDs [23] and in a phenomenological model of proton GPDs [24].

Electric charge and magnetization densities in the transverse plane also provide insights into the structure of the nucleons. The charge and magnetization densities in the transverse plane are defined as the Fourier transform of the electromagnetic form factors. The form factors involve initial and final states with different momenta and the three dimensional Fourier transforms cannot be interpreted as densities whereas the transverse densities (i.e., Fourier transformed only for the transverse momenta) defined at fixed light-front time are free from this difficulty and have a proper density interpretation [25,26]. We calculate the transverse charge and anomalous magnetization densities for both proton and neutron in the light-front diquark model and compare with the two different global parameterizations proposed by Kelly [27] and Bradford et al. [28]. We present results for both unpolarized and transversely polarized nucleons. We also present a comparison with the AdS/QCD results [29] for the transverse charge and magnetization densities.

This paper is organized as follows. In Sect. 2, we give brief introductions to the nucleon LFWFs of the quark–diquark model as well as the electromagnetic flavor form factors. We show the results for proton GPDs of u- and d-quarks in momentum space in Sect. 3. Then we discuss the GPDs in the transverse as well as the longitudinal impact parameter space in Sects. 3.1 and 3.2. We present the results of the charge and anomalous magnetization densities in the transverse plane in Sect. 4. Finally we provide a brief summary and conclusions in Sect. 5. For GPDs with nonzero skewness, we present a comparison of the quark–diquark model results with a Double Distribution (DD) model in the appendix.

2 Light-front quark–diquark model for the nucleon

In the quark–scalar diquark model, the three valence quarks of the nucleon are considered as an effectively composite system composed of a fermion and a neutral scalar bound state of diquark based on one loop quantum fluctuations. In the light-cone formalism for a spin $\frac{1}{2}$ composite system the Dirac and Pauli form factors $F_1(q^2)$ and $F_2(q^2)$ are identified with the helicity-conserving and helicity-flip matrix elements of the J^+ current [30],

$$\left\langle P+q,\uparrow\left|\frac{J^+(0)}{2P^+}\right|P,\uparrow\right\rangle = F_1(q^2), \tag{1}$$

$$\left\langle P+q,\uparrow\left|\frac{J^+(0)}{2P^+}\right|P,\downarrow\right\rangle = -(q^1-iq^2)\frac{F_2(q^2)}{2M_n}, \tag{2}$$

here M_n is the nucleon mass. Writing the proton as a two particle bound state of a quark and a scalar diquark in the light-front quark–diquark model, the Dirac and Pauli form factors for the quarks can be written in the light-front representation [30–33] as

$$F_1^q(Q^2) = \int_0^1 \mathrm{d}x \int \frac{\mathrm{d}^2\mathbf{k}_\perp}{16\pi^3}\,[\psi_{+q}^{+*}(x,\mathbf{k}'_\perp)\psi_{+q}^{+}(x,\mathbf{k}_\perp) + \psi_{-q}^{+*}(x,\mathbf{k}'_\perp)\psi_{-q}^{+}(x,\mathbf{k}_\perp)], \tag{3}$$

$$F_2^q(Q^2) = -\frac{2M_n}{q^1-iq^2}\int_0^1 \mathrm{d}x \int \frac{\mathrm{d}^2\mathbf{k}_\perp}{16\pi^3} [\psi_{+q}^{+*}(x,\mathbf{k}'_\perp)\psi_{+q}^{-}(x,\mathbf{k}_\perp) + \psi_{-q}^{+*}(x,\mathbf{k}'_\perp)\psi_{-q}^{-}(x,\mathbf{k}_\perp)], \tag{4}$$

where $\mathbf{k}'_\perp = \mathbf{k}_\perp + (1-x)\mathbf{q}_\perp$. $\psi^{\lambda_N}_{\lambda_q q}(x,\mathbf{k}_\perp)$ are the LFWFs with specific nucleon helicities $\lambda_N = \pm$ and for the struck quark $\lambda_q = \pm$, where the plus and minus correspond to $+\frac{1}{2}$ and $-\frac{1}{2}$, respectively. We consider the frame where $q = (0, 0, \mathbf{q}_\perp)$, thus $Q^2 = -q^2 = \mathbf{q}_\perp^2$.

We adopt the generic ansatz for the quark–diquark model of the valence Fock state of the nucleon LFWFs at an initial scale $\mu_0 = 313$ MeV as proposed in [1]:

$$\begin{aligned}
\psi_{+q}^{+}(x,\mathbf{k}_\perp) &= \varphi_q^{(1)}(x,\mathbf{k}_\perp),\\
\psi_{-q}^{+}(x,\mathbf{k}_\perp) &= -\frac{k^1+ik^2}{xM_n}\,\varphi_q^{(2)}(x,\mathbf{k}_\perp),\\
\psi_{+q}^{-}(x,\mathbf{k}_\perp) &= \frac{k^1-ik^2}{xM_n}\,\varphi_q^{(2)}(x,\mathbf{k}_\perp),\\
\psi_{-q}^{-}(x,\mathbf{k}_\perp) &= \varphi_q^{(1)}(x,\mathbf{k}_\perp),
\end{aligned} \tag{5}$$

where $\varphi_q^{(1)}(x,\mathbf{k}_\perp)$ and $\varphi_q^{(2)}(x,\mathbf{k}_\perp)$ are the wave functions predicted by soft-wall AdS/QCD [34], modified by intro-

Table 1 The parameters in the model for $\kappa = 0.4066$ GeV

Parameters	u	d
$a^{(1)}$	0.035	0.20
$b^{(1)}$	0.080	1.00
$a^{(2)}$	0.75	1.25
$b^{(2)}$	−0.60	−0.20
$N^{(1)}$	29.180	33.918
$N^{(2)}$	1.459	1.413

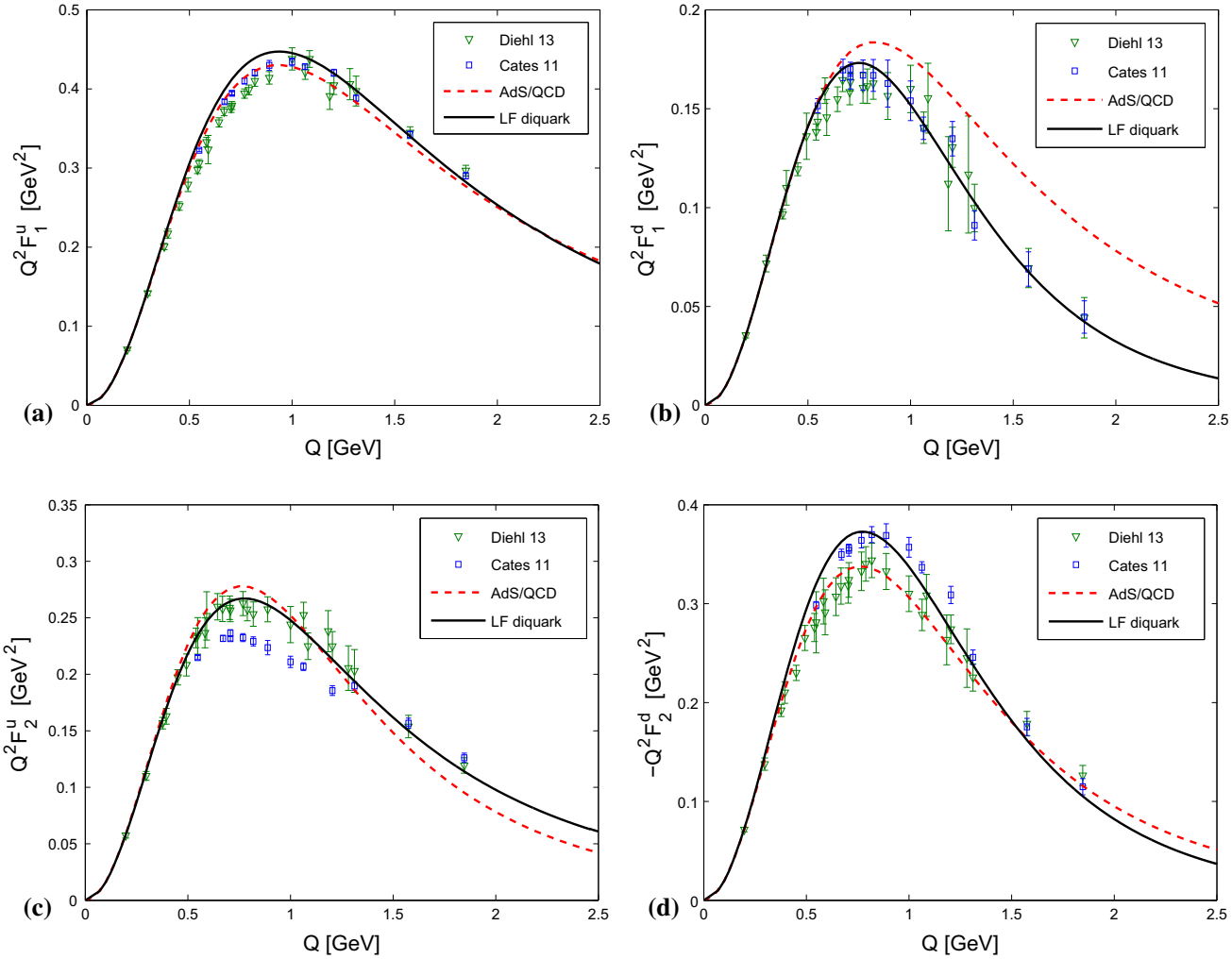

Fig. 1 Plots of flavor dependent form factors for u- and d-quarks. The experimental data are taken from [40,41]. The *red dashed lines* represent the soft-wall AdS/QCD model [35]

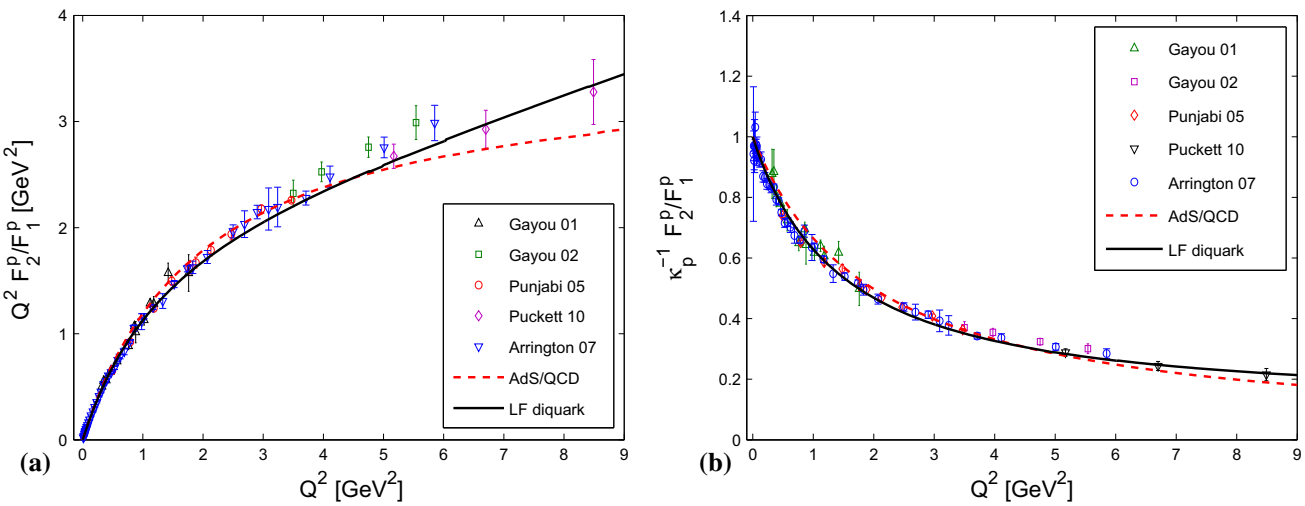

Fig. 2 Light-front quark–diquark model results are fitted with the experimental data. The plots show the ratio of Pauli and Dirac form factors for the proton, **a** the ratio is multiplied by $Q^2 = -q^2 = -t$, **b** the ratio is divided by κ_p. The experimental data are taken from Refs. [42–46]. The *red dashed lines* represent the soft-wall AdS/QCD model [35]

ducing the tunable parameters $a_q^{(i)}$ and $b_q^{(i)}$ for quark q [1]:

$$\varphi_q^{(i)}(x,\mathbf{k}_\perp) = N_q^{(i)}\frac{4\pi}{\kappa}\sqrt{\frac{\log(1/x)}{1-x}}\,x^{a_q^{(i)}}(1-x)^{b_q^{(i)}} \times \exp\left[-\frac{\mathbf{k}_\perp^2}{2\kappa^2}\frac{\log(1/x)}{(1-x)^2}\right]. \quad (6)$$

The parameters are tuned to fit the electromagnetic properties of the nucleons. Following the convention of [1], we fix the normalizations of the Dirac and Pauli form factors as

$$F_1^q(Q^2) = n_q\frac{I_1^q(Q^2)}{I_1^q(0)}, \quad F_2^q(Q^2) = \kappa_q\frac{I_2^q(Q^2)}{I_2^q(0)}, \quad (7)$$

so that $F_1^q(0) = n_q$ and $F_2^q(0) = \kappa_q$ where $n_u = 2$, $n_d = 1$ and the anomalous magnetic moments for the u- and d-quarks are $\kappa_u = 1.673$ and $\kappa_d = -2.033$. The advantage of the modified formulas in Eq. (7) is that, irrespective of the values of the parameters, the normalization conditions for the form factors are automatically satisfied. The structure integrals, $I_i^q(Q^2)$, have the form

$$I_1^q(Q^2) = \int_0^1 \mathrm{d}x\,x^{2a_q^{(1)}}(1-x)^{1+2b_q^{(1)}}R_q(x,Q^2) \times \exp\left[-\frac{Q^2}{4\kappa^2}\log(1/x)\right], \quad (8)$$

$$I_2^q(Q^2) = 2\int_0^1 \mathrm{d}x\,x^{2a_q^{(1)}-1}(1-x)^{2+2b_q^{(1)}}\sigma_q(x) \times \exp\left[-\frac{Q^2}{4\kappa^2}\log(1/x)\right], \quad (9)$$

with

$$R_q(x,Q^2) = 1+\sigma_q^2(x)\frac{(1-x)^2}{x^2}\frac{\kappa^2}{M_n^2\log(1/x)} \times\left[1-\frac{Q^2}{4\kappa^2}\log(1/x)\right],$$

$$\sigma_q(x) = \frac{N_q^{(2)}}{N_q^{(1)}}x^{a_q^{(2)}-a_q^{(1)}}(1-x)^{b_q^{(2)}-b_q^{(1)}}. \quad (10)$$

It is straightforward to write down the flavor decompositions of the Dirac and Pauli form factors of the nucleon as

$$F_i^{p(n)} = e_u F_i^{u(d)} + e_d F_i^{d(u)} \quad (i=1,2) \quad (11)$$

where e_u and e_d are the charges of u- and d-quarks in units of the positron charge (e). On top of the AdS/QCD scale parameter κ, the wave functions involve four more parameters $a_q^{(i)}$ and $b_q^{(i)}$ (with $i = 1, 2$) for each quark. In Ref. [1], κ is taken to be 0.35 GeV and the parameters are evaluated to fit the electromagnetic properties of the nucleon. But the results for the form factors presented in that paper are not converging with respect to the lower limit of x integrations in Eqs. (8 and 9). The comparisons with experimental data presented in several plots in Ref. [1] are true only for an unrealistically large value of lower limit for the x integrations which drastically change when integrated from $x \to 0$. So, when proper limits in the x-integrations are taken, the parameters presented in [1] cannot reproduce the data. In this work, we use a different scale parameter $\kappa = 0.4066$ GeV, which was obtained by fitting the nucleon form factors in the AdS/QCD soft-wall model [14,35]. Here, we show that we can reproduce the nucleon form factors with the new parameters $a_q^{(i)}$, $b_q^{(i)}$, and $N^{(i)}$ listed in Table 1. The results are stable and converging under the integration over x. The new parameters reproduce the experimental data quite accurately for a wide range of Q^2 values.

The Dirac and Pauli form factors of both u- and d-quarks are shown in Fig. 1. The form factors F_1^q and F_2^q for both u- and d-quarks in light-front quark–diquark model for the scale parameter $\kappa = 0.4066$ GeV and the parameters defined in Table 1 are in excellent agreement with the data. For F_1^d, we can see a clear improvement in the quark–diquark model over the AdS/QCD model. It is important to note that other models fail to reproduce the form factors data for the d-quark [37]. In Fig. 2, we show the fit of the light-front quark–diquark model results with experimental data of proton form factors. We get excellent agreement with the data. In the same plots, we also

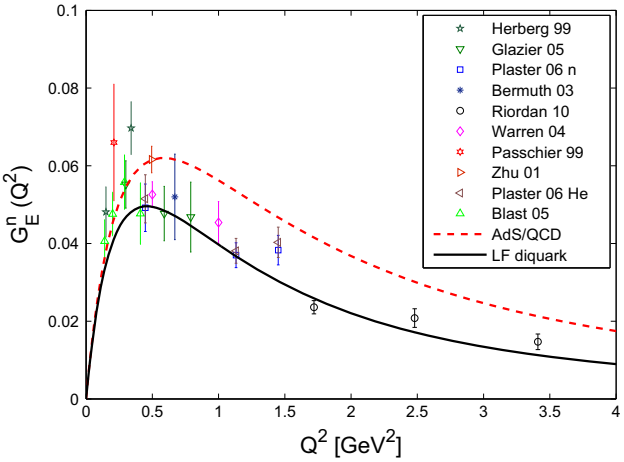

Fig. 3 The Sachs form factor $G_E^n(Q^2)$ for the neutron. The experimental data are taken from Refs. [47–55]. The *red dashed line* represents the soft-wall AdS/QCD model prediction

Table 2 Electromagnetic radii of the nucleons

Quantity	Our results	Measured data [36]
r_E^p (fm)	0.7861	0.877 ± 0.005
r_M^p (fm)	0.7719	0.777 ± 0.016
$\langle r_E^2\rangle^n$ (fm^2)	-0.085	-0.1161 ± 0.0022
r_M^n (fm)	0.7596	$0.862^{+0.009}_{-0.008}$

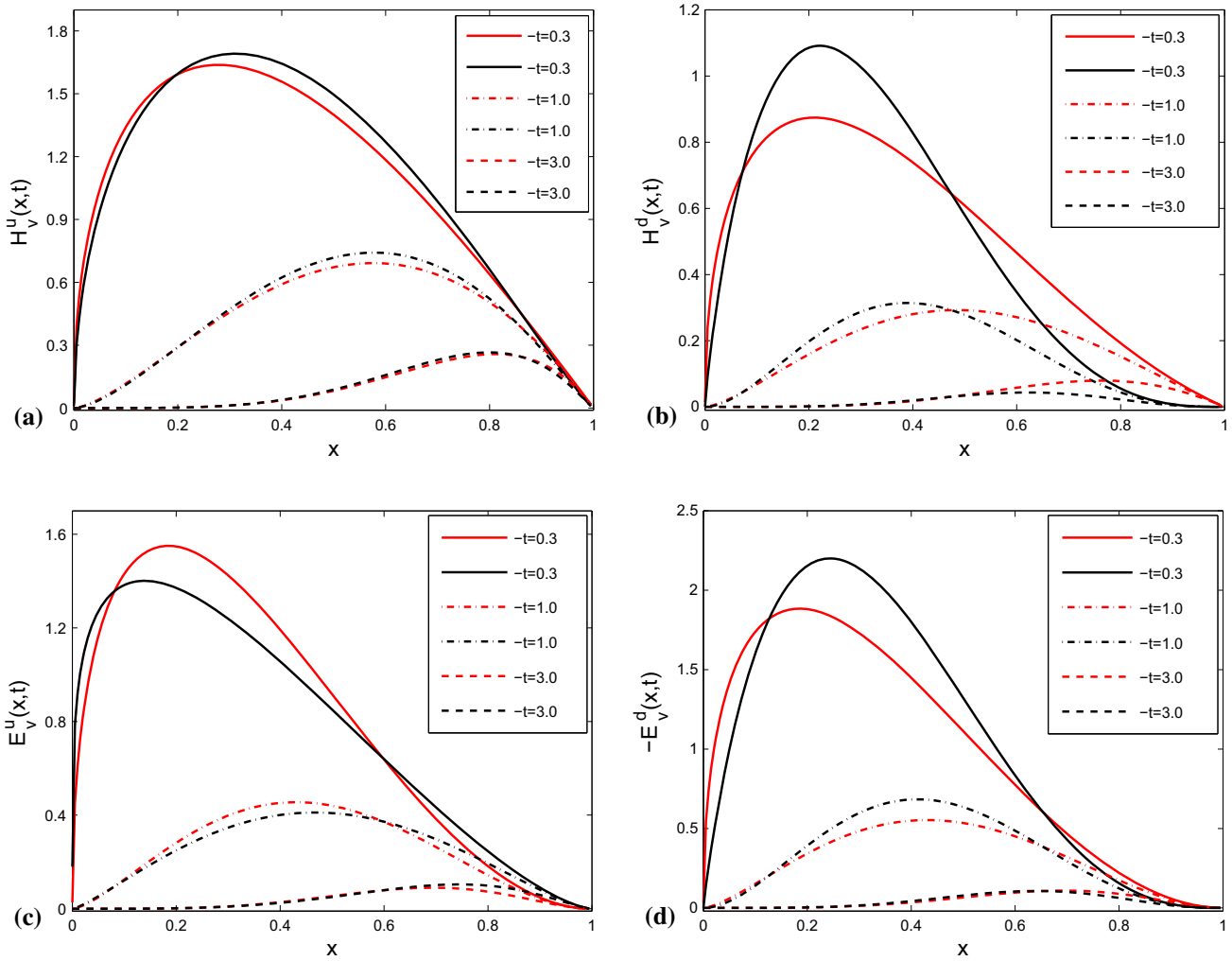

Fig. 4 Plots of GPDs $H^q(x,t)$ and $E^q(x,t)$ vs. x, for fixed values of $-t$. The *black lines* represent the light-front quark–diquark model, and the *red lines* are for AdS/QCD model [14]

show comparisons of the light-front quark–diquark model and the soft-wall AdS/QCD model with the same value of κ [35]. The results of the light-front quark–diquark model agree with the data better than AdS/QCD; specially at large Q^2 values we achieve substantial improvement. The Sachs form factor $G_E(Q^2)$ for the neutron is shown in Fig. 3. Again, our results agree with the experimental data much better than the AdS/QCD results. The fitted results for the electromagnetic radii of the nucleons are listed in Table 2. The standard formulas for the electromagnetic radii of the nucleon used here are given below:

$$\langle r_E^2\rangle^N = -6\frac{\mathrm{d}G_E^N(Q^2)}{\mathrm{d}Q^2}\Big|_{Q^2=0}, \tag{12}$$

$$\langle r_M^2\rangle^N = -\frac{6}{G_M^N(0)}\frac{\mathrm{d}G_M^N(Q^2)}{\mathrm{d}Q^2}\Big|_{Q^2=0} \tag{13}$$

where N stands for the nucleon ($N = p/n$) and the Sachs form factors are defined as

$$G_E^N(Q^2) = F_1^N(Q^2) - \frac{Q^2}{4M_N^2}F_2^N(Q^2), \tag{14}$$

$$G_M^N(Q^2) = F_1^N(Q^2) + F_2^N(Q^2). \tag{15}$$

3 Generalized parton distributions

Using the overlap formalism of light-front wave functions, we evaluate the GPDs in light-front quark–diquark model. We consider the DGLAP domain, i.e., $\zeta < x < 1$ where ζ is the skewness and x is the light-front longitudinal momentum fraction carried by the struck quark. This domain corresponds to the situation where one removes a quark from the initial proton with light-front momentum fraction $x = \frac{k^+}{P^+}$ and the

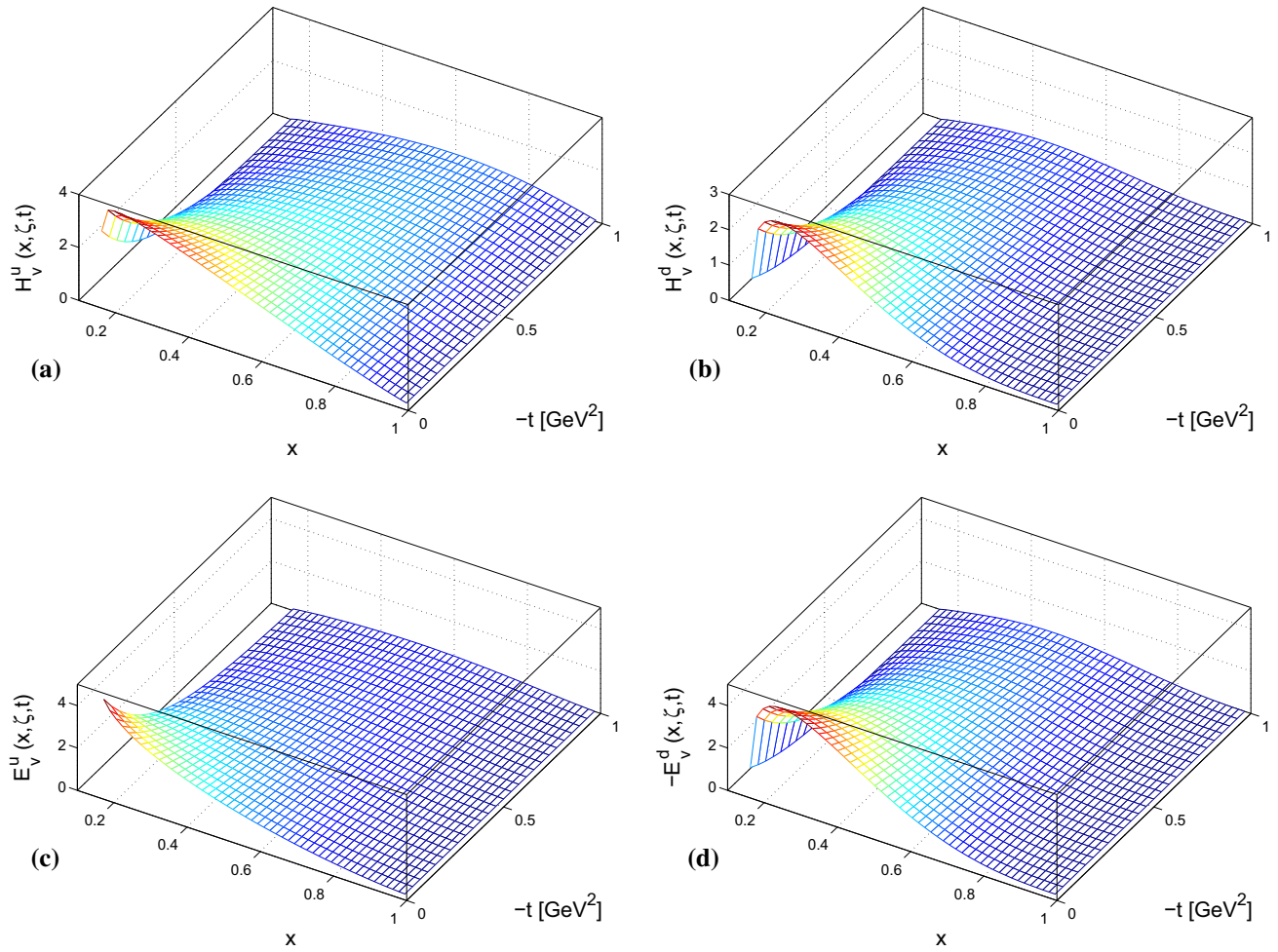

Fig. 5 Plots of $H^q(x,\zeta,t)$ and $E^q(x,\zeta,t)$ vs. x and $-t$ for a fixed value of $\zeta = 0.15$. For $\zeta = 0.15$, the minimum value of $-t \approx 0.024$ GeV^2

transverse momentum $\mathbf{k}_\perp$ and re-inserts it into the final state of the proton with longitudinal momentum fraction $x-\zeta$ and transverse momentum $\mathbf{k}_\perp - \mathbf{q}_\perp$. The contributions to the GPDs for $0 < x < \zeta$ come from the particle number changing interactions and cannot be studied in this model. The kinematical domain for the GPDs studied here is thus restricted to $\zeta < x < 1$ where only diagonal overlaps (2-particle state $\to$ 2-particle state) contribute. The GPDs H and E are defined through the matrix element of the bilocal vector current on the light-front:

$$\int \frac{\mathrm{d}y^-}{8\pi} \mathrm{e}^{ixP^+y^-/2} \langle P',\lambda'|\,\bar{\psi}(0)\gamma^+\psi(y)\,|P,\lambda\rangle = \frac{1}{2P^+}\bar{U}(P',\lambda')\left[H(x,\zeta,t)\gamma^+ E(x,\zeta,t)\frac{i}{2M_n}\sigma^{+\alpha}q_\alpha\right]U(P,\lambda). \tag{16}$$

The proton state $|\,P,\lambda\rangle$ is written in two particle Fock states with one fermion and a scalar boson in the light-front quark–diquark model. Using the relations

$$\frac{1}{2\bar{P}^+}\bar{U}(P',\lambda')\gamma^+U(P,\lambda) = \frac{\sqrt{1-\zeta}}{1-\frac{\zeta}{2}}\,\delta_{\lambda,\lambda'},$$
$$\frac{1}{2\bar{P}^+}\bar{U}(P',\lambda')\frac{i}{2M_n}\sigma^{+\alpha}q_\alpha U(P,\lambda) = -\frac{\zeta^2}{4(1-\frac{\zeta}{2})\sqrt{1-\zeta}}\,\delta_{\lambda,\lambda'} + \frac{1}{\sqrt{1-\zeta}}\,\frac{\lambda q^1 + iq^2}{2M_n}\,\delta_{\lambda,-\lambda'}, \tag{17}$$

where $\bar{P} = (P+P')/2$ and $\lambda(\lambda') = \pm\frac{1}{2}$ is the initial (final) proton spin, we have the following expressions for the GPDs in terms of the LFWFs in the quark–diquark model:

$$\frac{\sqrt{1-\zeta}}{1-\frac{\zeta}{2}}\,H_v^q(x,\zeta,t) - \frac{\zeta^2}{4(1-\frac{\zeta}{2})\sqrt{1-\zeta}}\,E_v^q(x,\zeta,t) = \int \frac{\mathrm{d}^2\mathbf{k}_\perp}{16\pi^3}\,[\psi_{+q}^{+*}(x',\mathbf{k}'_\perp)\psi_{+q}^{+}(x,\mathbf{k}_\perp) + \psi_{-q}^{+*}(x',\mathbf{k}'_\perp)\psi_{-q}^{+}(x,\mathbf{k}_\perp)] \tag{18}$$

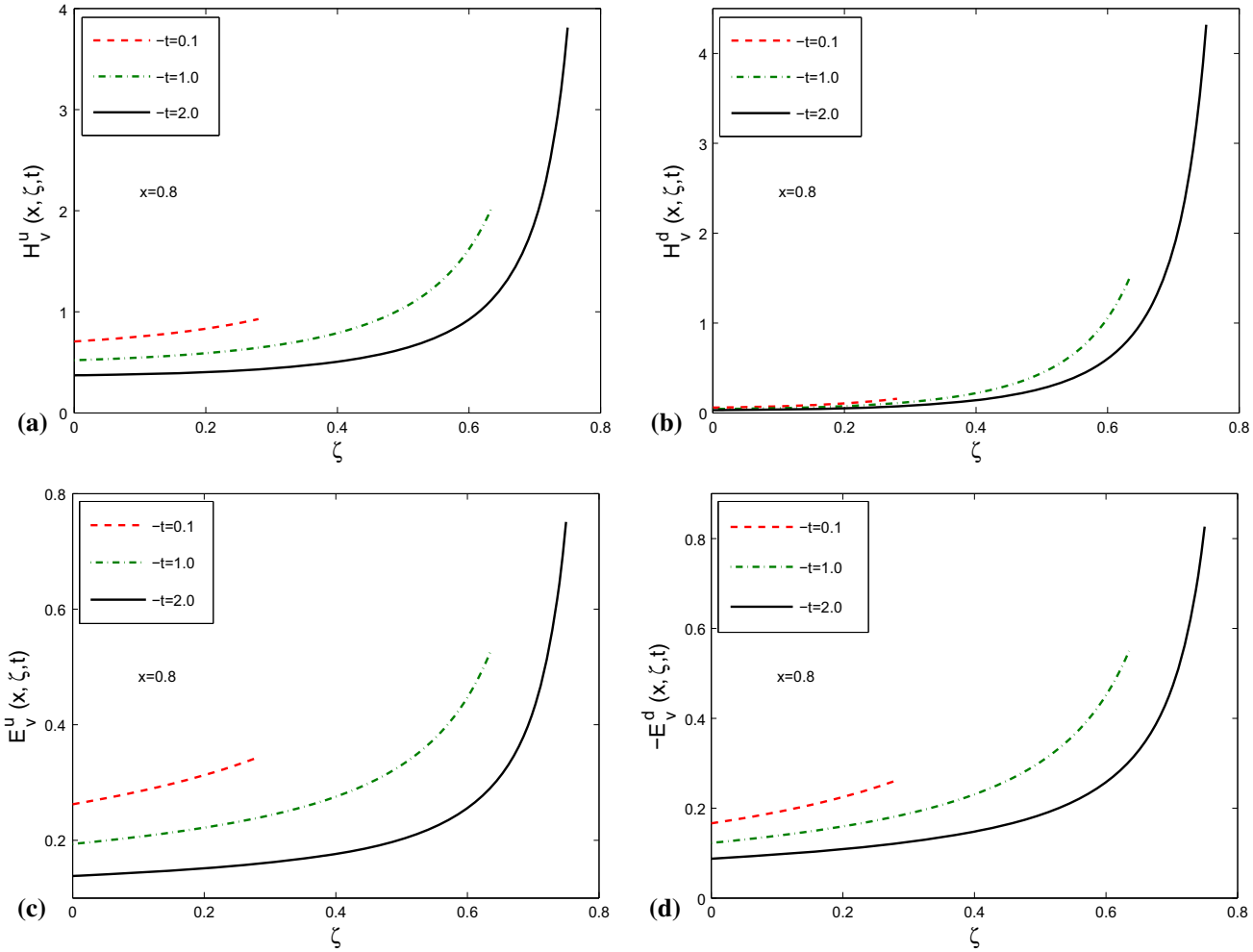

Fig. 6 Plots of $H^q(x,\zeta,t)$ and $E^q(x,\zeta,t)$ vs. ζ for a fixed value of $x = 0.8$

and

$$\frac{1}{\sqrt{1-\zeta}}\,\frac{-(q^1-iq^2)}{2M_n}\,E_v^q(x,\zeta,t) = \int \frac{\mathrm{d}^2\mathbf{k}_\perp}{16\pi^3}\,[\psi_{+q}^{+*}(x',\mathbf{k}'_\perp)\psi_{+q}^{-}(x,\mathbf{k}_\perp) + \psi_{-q}^{+*}(x',\mathbf{k}'_\perp)\psi_{-q}^{-}(x,\mathbf{k}_\perp)], \tag{19}$$

where

$$x' = \frac{x-\zeta}{1-\zeta}, \quad \mathbf{k}'_\perp = \mathbf{k}_\perp - \frac{1-x}{1-\zeta}\,\mathbf{q}_\perp. \tag{20}$$

Substituting the LFWFs (Eq. 5) in Eqs. (18) and (19) and integrating over $\mathbf{k}_\perp$, we get the following expressions for the GPDs:

$$E_v^q(x,\zeta,t) = \kappa_q\,\frac{\mathcal{F}_2^q(x,\zeta,t)}{I_2^q(0)}, \tag{21}$$

$$H_v^q(x,\zeta,t) = n_q\,\frac{1-\frac{\zeta}{2}}{I_1^q(0)\sqrt{1-\zeta}} \times\left[\mathcal{F}_1^q(x,\zeta,t) + \frac{\zeta^2}{4(1-\frac{\zeta}{2})\sqrt{1-\zeta}}\,E_v^q(x,\zeta,t)\right]. \tag{22}$$

The functions $\mathcal{F}_i^q(x,\zeta,t)$ are given by

$$\mathcal{F}_1^q(x,\zeta,t) = \frac{1}{\kappa^2}\sqrt{\frac{\log(1/x)}{(1-x)}}\sqrt{\frac{\log(1/x')}{(1-x')}}\Bigg[(xx')^{a_q^{(1)}} ((1-x)(1-x'))^{b_q^{(1)}}\frac{1}{A} + \left[\frac{N_q^{(2)}}{N_q^{(1)}}\right]^2\frac{1}{M_n^2}((xx')^{a_q^{(2)}-1} ((1-x)(1-x'))^{b_q^{(2)}}\left(\frac{1}{A^2} - \frac{(1-x')^2Q^2}{4}\frac{1}{A} + Q^2\left(\frac{\log(1/x')}{2\kappa^2(1-x')A} - \frac{1-x'}{2}\right)^2\frac{1}{A}\right)\Bigg]$$

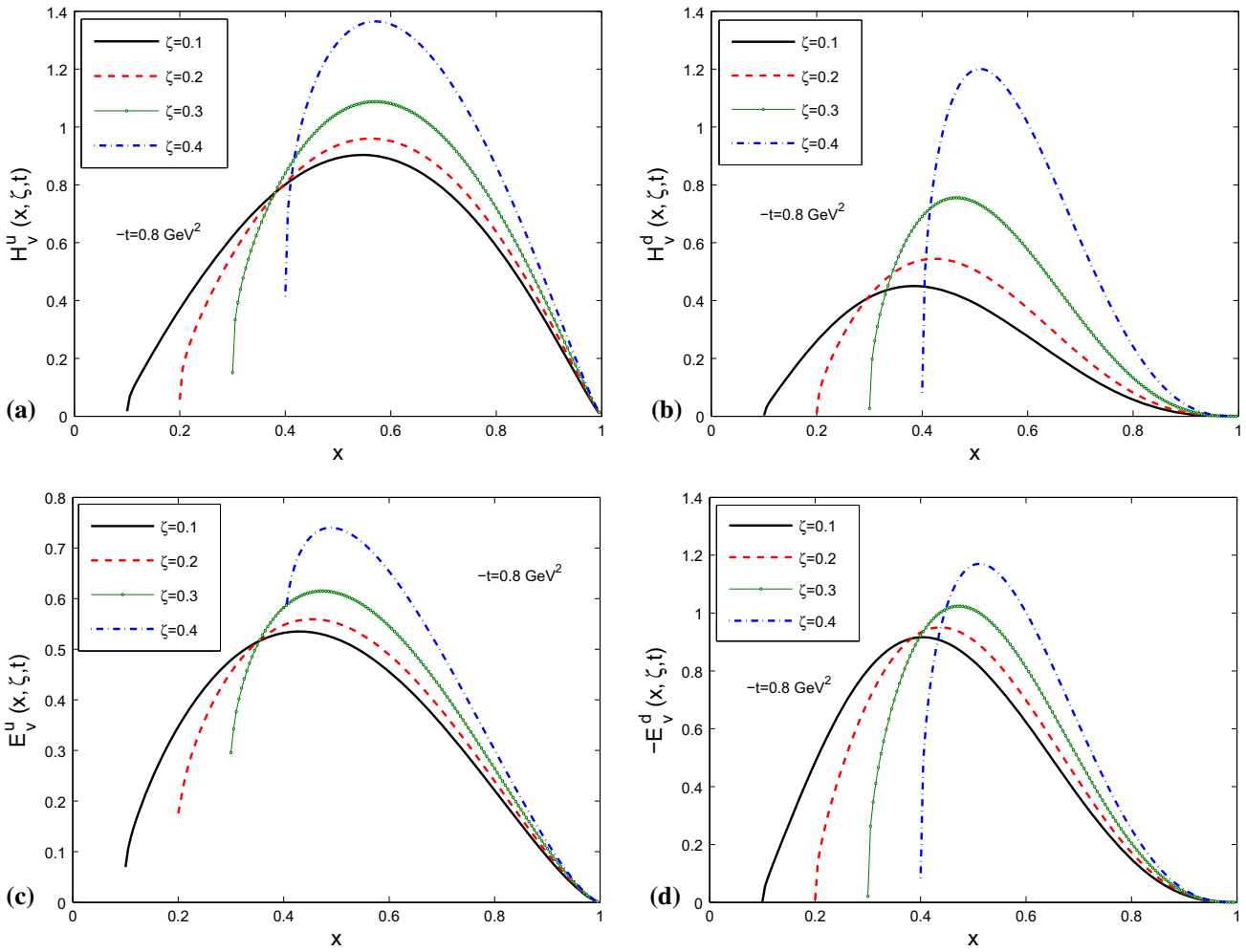

Fig. 7 Plots of $H^q(x,\zeta,t)$ and $E^q(x,\zeta,t$ vs. x, for a fixed value of $-t = 0.8$ GeV^2 and different values of ζ

$$\times \exp\left[\frac{\log(1/x')}{2\kappa^2} Q^2\left(\frac{\log(1/x')}{2\kappa^2(1-x')^2 A} - 1\right)\right], \tag{23}$$

$$\begin{aligned}\mathcal{F}_2^q(x,\zeta,t) = {} & \frac{2\sqrt{1-\zeta}}{\kappa^2}\frac{N_q^{(2)}}{N_q^{(1)}}\sqrt{\frac{\log(1/x)}{(1-x)}}\sqrt{\frac{\log(1/x')}{(1-x')}} \\ & \times\left[\frac{\log(1/x')}{2\kappa^2(1-x')A}(x'^{a_q^{(1)}} x^{a_q^{(2)}-1}(1-x')^{b_q^{(1)}}(1-x)^{b_q^{(2)}}\right. \\ & -x^{a_q^{(1)}} x'^{a_q^{(2)}-1}(1-x)^{b_q^{(1)}}(1-x')^{b_q^{(2)}}) \\ & \left.+x^{a_q^{(1)}} x'^{a_q^{(2)}-1}(1-x)^{b_q^{(1)}}(1-x')^{b_q^{(2)}+1}\right]\frac{1}{A} \\ & \times\exp\left[\frac{\log(1/x')}{2\kappa^2} Q^2\left(\frac{\log(1/x')}{2\kappa^2(1-x')^2 A} - 1\right)\right],\end{aligned} \tag{24}$$

where $Q^2 = -t(1-\zeta) - M_n^2\zeta^2$ and A is a function of x and x':

$$A = A(x,x') = \frac{\log(1/x)}{2\kappa^2(1-x)^2} + \frac{\log(1/x')}{2\kappa^2(1-x')^2}. \tag{25}$$

$I_1^q(0)$ and $I_2^q(0)$ are the integrals defined in Eqs. (8) and (9) for $Q^2 = 0$. The GPDs are normalized as

$$\begin{aligned}\int_0^1 \mathrm{d}x\, H^q(x,0,0) &= n_q, \\ \int_0^1 \mathrm{d}x\, E^q(x,0,0) &= \kappa_q,\end{aligned} \tag{26}$$

where n_q denotes the number of u or d valence quarks in the proton and the quark anomalous magnetic moment is denoted by κ_q. According to the polynomiality condition, the nth Mellin moment of a GPD should be a polynomial with highest power ζ^n at $t \to 0$ [38,39]. Since the moments require the GPDs for all values of $-1 \le x \le 1$, it is not possible to confirm the polynomiality condition in this model as the GPDs are evaluated only for $0 \le \zeta < x$. But we have numerically checked for $n = 1, 2, 3$, and 4 that the moments $\int_\zeta^1 x^{n-1} H(x,\zeta,t)$ show a behavior consistent with the polynomiality condition in the limit $t \to 0$.

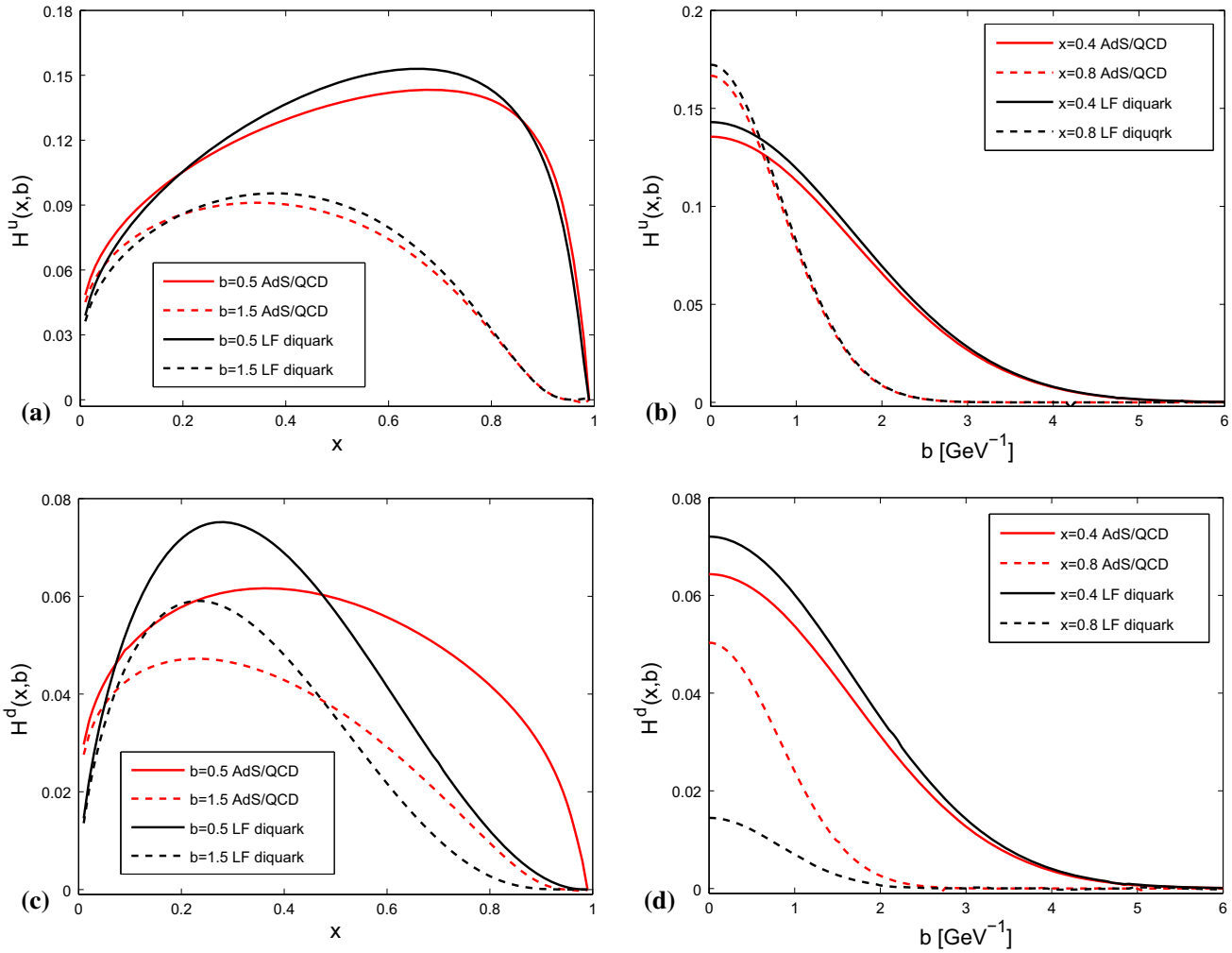

Fig. 8 $H^q(x, \mathbf{b}_\perp)$ plotted against x and $b = |\ \mathbf{b}_\perp\ |$. b is in GeV^{-1}

The GPDs for zero skewness($\zeta = 0$) in light-front quark–diquark model are compared with the AdS/QCD results [14] in Fig. 4. In Fig. 4a and b, we show the GPD $H(x, t)$ as a function of x for different values of $-t$ for u- and d-quarks. Similar plots of $E(x, t)$ for u- and d-quarks are shown in Fig. 4c and d. The overall nature of both models is same for the u-quark while there is some disagreement in the GPD $H(x, t)$ for the d-quark. Since the d-quark form factors are not well described in AdS/QCD, this disagreement is expected. The GPD $H(x, t)$ falls off faster as x increases for the d-quark compare to u-quark in both models. Unlike $H(x, t)$, the fall-off of the GPD $E(x, t)$ at large x is similar for both u- and d-quarks with increasing x.

In Fig. 5, we show the skewness dependent GPDs as a function of x and t for a fixed $\zeta = 0.15$. The overall behaviors of the GPDs with nonzero ζ are similar to the zero skewness GPDs. The same GPDs for a fixed $x = 0.8$ are shown as a function of ζ for different values of $-t$ in Fig. 6. In Fig. 7a and b we have plotted the GPD $H(x, \zeta, t)$ as a function of x for u and d-quarks for different values of ζ with fixed value of $-t = 0.8$ GeV^2. The similar plots of $E(x, \zeta, t)$ for u- and d quarks are shown in Fig. 7c and d. In Fig. 7, the peaks of all the distributions move to higher x as ζ increases and the amplitudes of the distributions increase with increasing ζ for a fixed value of $-t$. Due to the factor of $\sqrt{1-\zeta}$ in the denominator of the GPD $H(x, \zeta, t)$ in Eq. (22), the increase in the magnitude with increasing ζ is more in $H(x, \zeta, t)$ than in $E(x, \zeta, t)$.

3.1 GPDs in transverse impact parameter space

GPDs in transverse impact parameter space are defined as [8,56,57]:

$$H(x, \zeta, \mathbf{b}_\perp) = \frac{1}{(2\pi)^2} \int \mathrm{d}^2\mathbf{q}_\perp \mathrm{e}^{-i\mathbf{q}_\perp \cdot \mathbf{b}_\perp} H(x, \zeta, t),$$

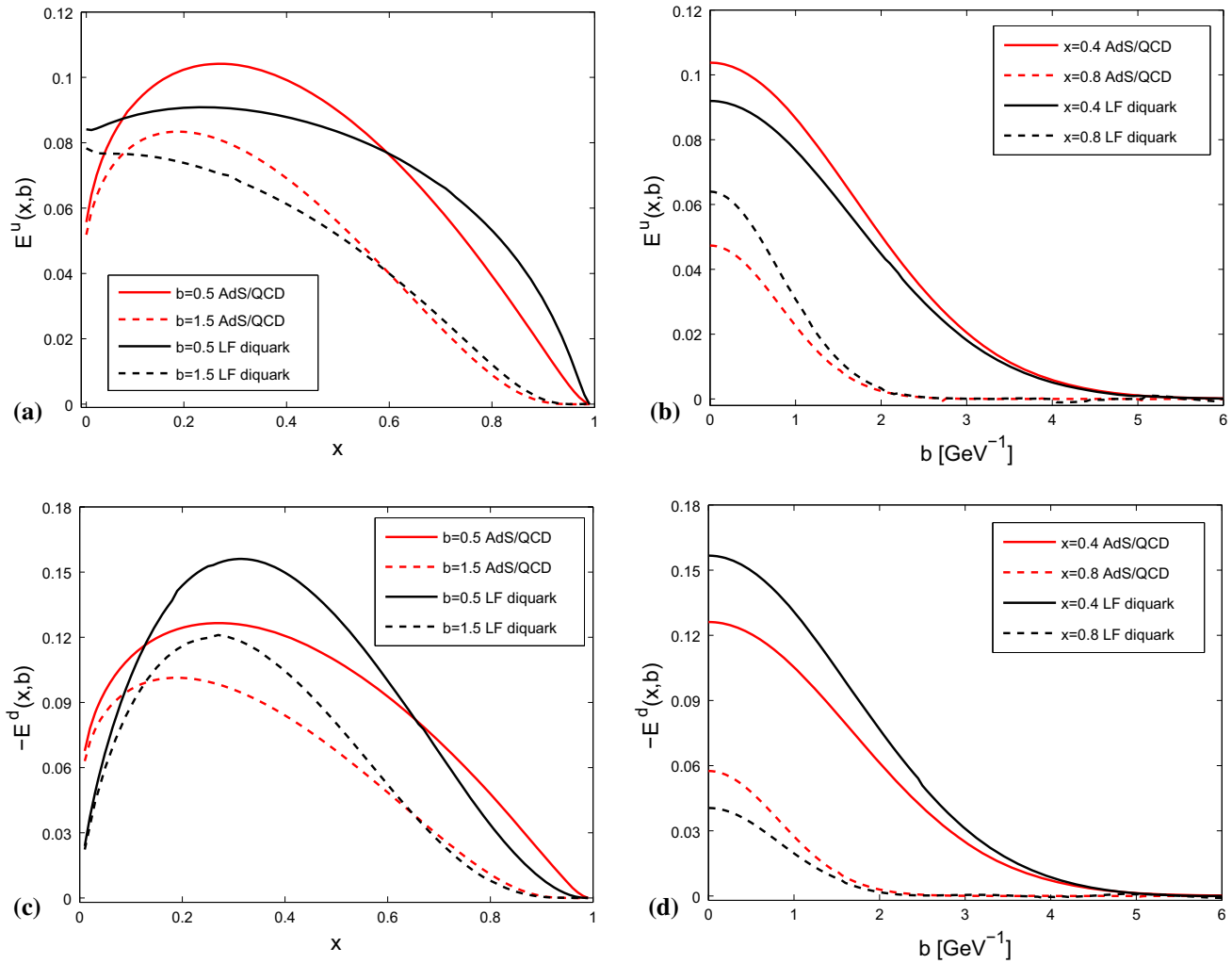

Fig. 9 $E^q(x, \mathbf{b}_\perp)$ plotted against x and $b = |\mathbf{b}_\perp|$. b is in GeV^{-1}

$$E(x, \zeta, \mathbf{b}_\perp) = \frac{1}{(2\pi)^2} \int \mathrm{d}^2\mathbf{q}_\perp \mathrm{e}^{-i\mathbf{q}_\perp \cdot \mathbf{b}_\perp} E(x, \zeta, t). \tag{27}$$

Here, $\mathbf{b}_\perp$ is the transverse impact parameter. For zero skewness, $\mathbf{b}_\perp$ gives a measure of the transverse distance between the struck parton and the center of momentum of the hadron. $\mathbf{b}_\perp$ satisfies the condition $\sum_i x_i b_{\perp i} = 0$, where the sum is over the number of partons. The relative distance between the struck parton and the center of momentum of the spectator system is given by $\frac{|\mathbf{b}_\perp|}{1-x}$, which provides us an estimate of the size of the bound state [58]. However, the exact estimation of the nuclear size is not possible as the spatial extension of the spectator system is not available from the GPDs. In the DGLAP domain $x > \zeta$, the impact parameter $\mathbf{b}_\perp$ implies the location where the quark is pulled out and pushed back to the nucleon. In the ERBL region, $x < \zeta$, $\mathbf{b}_\perp$ gives the transverse location of the quark–antiquark pair inside the nucleon.

In Fig. 8, we compare the transverse impact parameter dependent proton GPD $H(x, \mathbf{b}_\perp)$ for zero skewness in the light-front quark–diquark model and in the soft-wall AdS/QCD case. Unlike $H^d(x, \mathbf{b}_\perp)$, the diquark model results for $H^u(x, \mathbf{b}_\perp)$ are in good agreement with AdS/ QCD. The GPD $H^d(x, \mathbf{b}_\perp)$ fall off slowly for large x in AdS/QCD compared to the diquark model, while the fall-off of $H^u(x, \mathbf{b}_\perp)$ in both models is the same. The reason of the disagreement in $H^d(x, \mathbf{b}_\perp)$ is that the AdS/QCD model is unable to reproduce F_1^d to match with experimental data whereas the form factor in the diquark model agrees well with the data (see Fig. 1b). The overall shapes of the curves in Fig. 8a and c are due to the fact that the two particle LFWFs are effectively functions of the "x-weighted transverse variable" [34] $z = \sqrt{x(1-x)}|b_\perp|$, which is true for both the AdS/QCD and the diquark models. Both models lack the symmetry about $x \to (1-x)$, the asymmetry is more prominent for the d-quark, in the diquark model due to the parameters $a_q^{(i)} \neq b_q^{(i)}$ in the diquark wave functions. In Fig. 9 we compare the two models for the proton GPD $E(x, \mathbf{b}_\perp)$. The GPD $E(x, \mathbf{b}_\perp)$ in

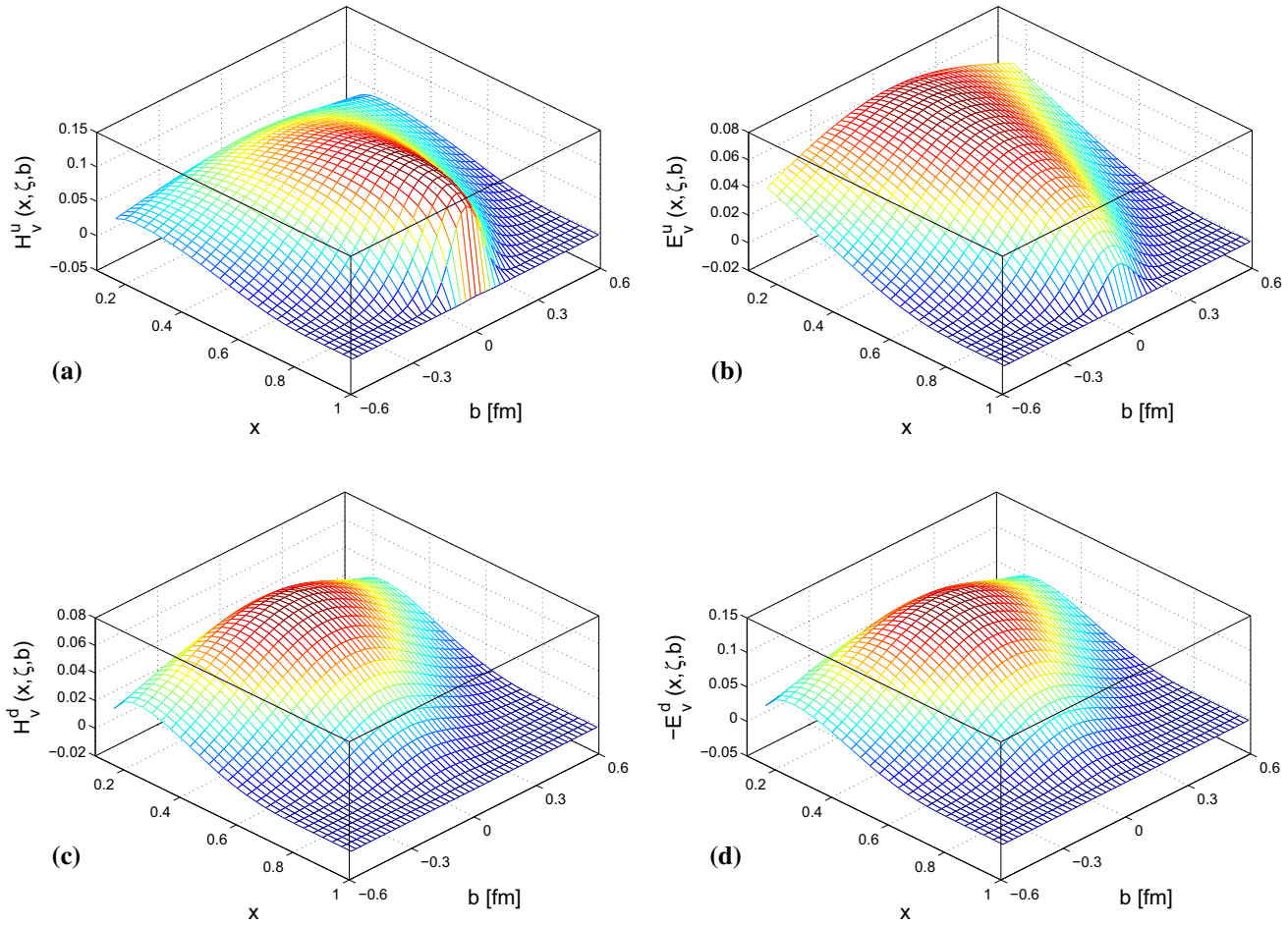

Fig. 10 Plots of $H^q(x, \zeta, \mathbf{b}_\perp)$ and $E^q(x, \zeta, \mathbf{b}_\perp)$ vs. x and $b = |\mathbf{b}_\perp|$, for a fixed value of $x = 0.15$

impact parameter space in the models are similar in behavior for both u- and d-quarks, though the agreement in the magnitudes is not exact. In AdS/QCD, the nature of $E(x, \mathbf{b}_\perp)$ for u- and d-quarks is almost similar when plotted against x for fixed values of the impact parameter $b = |\mathbf{b}_\perp|$, whereas in the diquark model, it shows a quite different behavior for both u- and d-quarks. But the behaviors of $H(x, \mathbf{b}_\perp)$ with respect to x are distinctly different for u- and d-quarks in both models as can be seen in Fig. 8. It is interesting to note that in both cases, the GPD $H(x, \mathbf{b}_\perp)$ is larger for the u-quarks than d-quarks, whereas the magnitude of the GPD $E(x, \mathbf{b}_\perp)$ is marginally larger for the d-quarks than that for the u-quarks at small values of the impact parameter b. The similar behavior of the GPDs of a phenomenological model was observed in [59]. Another interesting feature of the behavior of all the GPDs is that the width of all the distributions in transverse impact parameter space decreases as x increases, which implies that the distributions are more localized near the center of momentum for higher values of x.

The skewness dependent GPDs in transverse impact parameter space for u- and d-quarks as functions of x and b are shown in Fig. 10 for a fixed value of $\zeta = 0.15$. Similarly, all GPDs as functions of ζ and b for a fixed value of $x = 0.6$ are shown in Fig. 11. Though there is no divergence at $x = \zeta$, in the numerical computations, the exact value of $x = \zeta$ has been omitted for technical reason. At small value of b, $H(x, \zeta, \mathbf{b}_\perp)$ decreases for the u-quark but increases for d-quark with increasing ζ, while $E(x, \zeta, \mathbf{b}_\perp)$ decreases with increasing ζ for both u- and d for a fixed value of x. For the fixed values x and low ζ, the peak of the u-quark is sufficiently large compared to d for $H(x, \zeta, \mathbf{b}_\perp)$ but for $E(x, \zeta, \mathbf{b}_\perp)$, d-quark is marginally large compared to the u-quark. Substantial differences are observed in both GPDs between u- and d-quarks when the GPDs are plotted against x for fixed values of ζ and b. $H^d(x, \zeta, b)$ seems to be nonzero at $x = \zeta$ in Fig. 11c, but it is due to the fact that $x = \zeta$ is not included in the plot. It goes to zero as $x \to \zeta$. It is interesting to note that the peaks of all the distributions

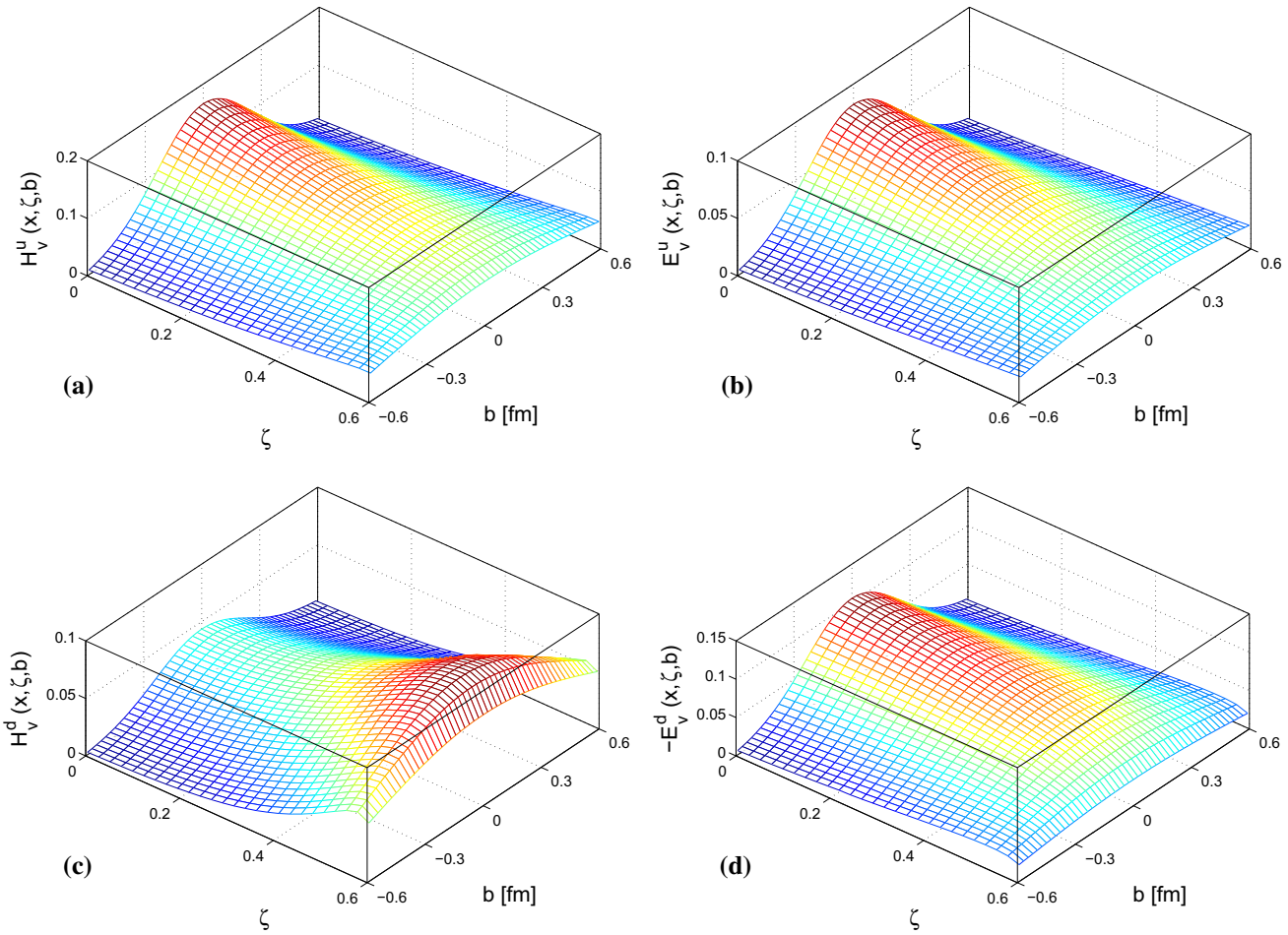

Fig. 11 Plots of $H^q(x,\zeta,\mathbf{b}_\perp)$ and $E^q(x,\zeta,\mathbf{b}_\perp)$ vs. ζ and $b = |\mathbf{b}_\perp|$, for a fixed value of $x = 0.6$

also become broader as ζ increases for a fixed value of x. This means that the probability of hitting the active quark at a larger transverse impact parameter b increases as the momentum transfer in the longitudinal direction increases.

3.2 GPDs in longitudinal impact parameter space

The boost invariant longitudinal impact parameter is defined as $\sigma = \frac{1}{2}b^- P^+$, which is conjugate to the skewness ζ, the measure of longitudinal momentum transfer. The parameter σ was first introduced in [21,22] and it was shown that the DVCS amplitude in a QED model of a dressed electron shows an interesting diffraction pattern in the longitudinal impact parameter space. Since Lorentz boosts are kinematical in the light front, the correlation defined in the three dimensional position space $b_\perp$ and σ is frame independent. It was shown in the same simple relativistic spin half system of an electron dressed with a photon that the GPDs also exhibit a similar diffraction pattern in the longitudinal impact parameter space [23]. A similar diffraction pattern was also observed in a phenomenological model for proton GPDs [24]. So, it is very interesting to investigate if a similar pattern is also observed in this light-front quark model. The GPDs in longitudinal position space are defined as

$$\begin{aligned} H(x,\sigma,t) &= \frac{1}{2\pi}\int_0^{\zeta_f} d\zeta e^{i\zeta P^+ b^-/2} H(x,\zeta,t), \\ &= \frac{1}{2\pi}\int_0^{\zeta_f} d\zeta e^{i\zeta\sigma} H(x,\zeta,t), \\ E(x,\sigma,t) &= \frac{1}{2\pi}\int_0^{\zeta_f} d\zeta e^{i\zeta P^+ b^-/2} E(x,\zeta,t), \\ &= \frac{1}{2\pi}\int_0^{\zeta_f} d\zeta e^{i\zeta\sigma} E(x,\zeta,t). \end{aligned} \tag{28}$$

Since we are considering the region $\zeta < x < 1$, the upper limit of ζ integration ζ_f is given by ζ_{max} if x is larger than ζ_{max}, otherwise by x if x is smaller than ζ_{max} where the maximum value of ζ for a fixed $-t$ is given by

$$\zeta_{max} = \frac{-t}{2M_n^2}\left(\sqrt{1+\frac{4M_n^2}{(-t)}} - 1\right). \tag{29}$$

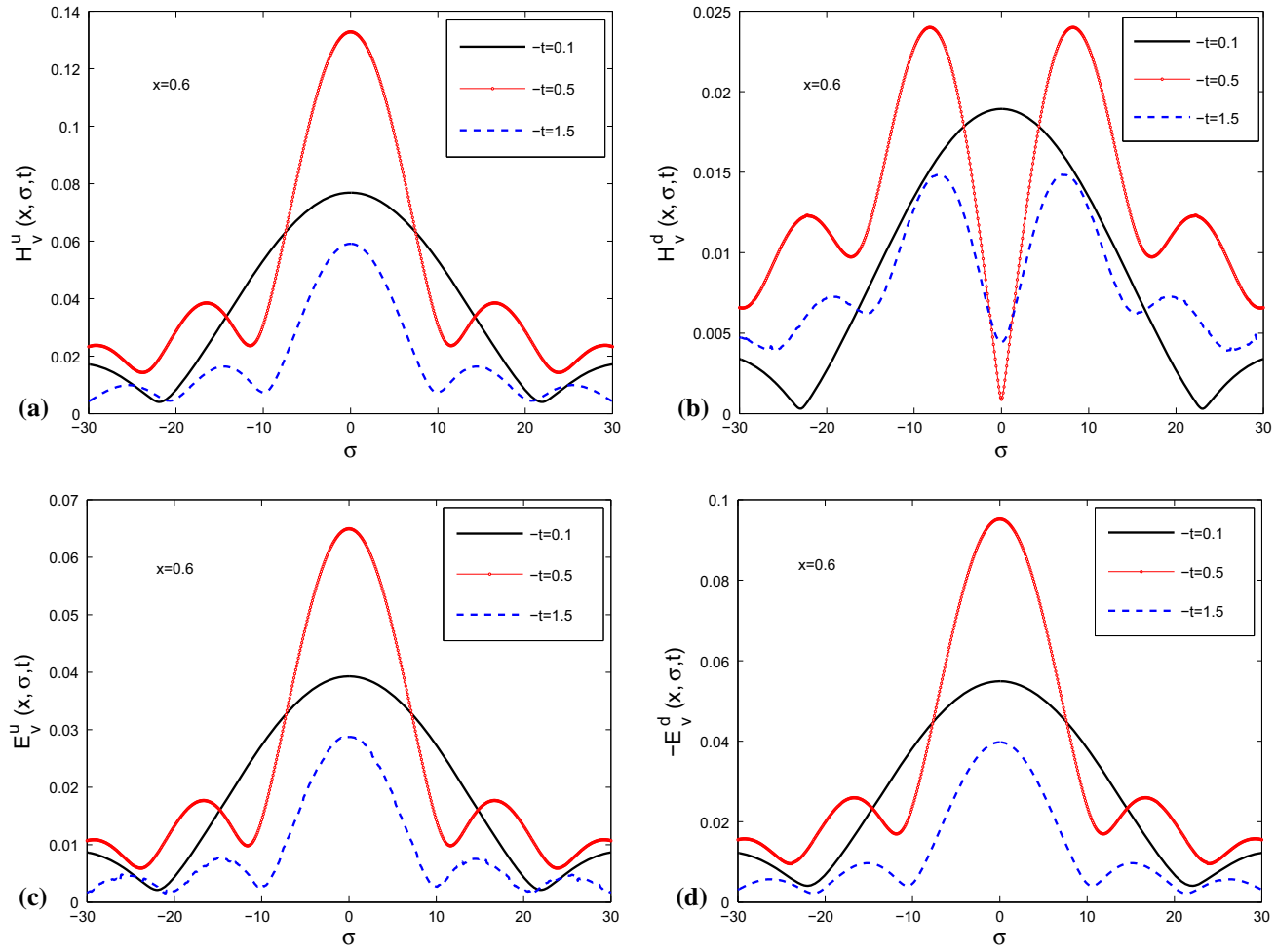

Fig. 12 GPDs in the longitudinal impact parameter space for a fixed value of $x = 0.6$ and different values of $-t$ ($-t$ is in GeV^2)

In Fig. 12, we show the GPDs in longitudinal position space σ considering the DGLAP region. We observe that the GPDs show a diffraction pattern in longitudinal impact parameter space, similar to the nature of a dressed electron in QED or in a holographic model for the meson [21,22]. This effect has also been observed for the GPDs of a phenomenological model [24] as well as for the chiral odd GPDs of light-front QED model [23]. Except for $H^d(x,\sigma,t)$, all the distributions have a primary maximum at $\sigma = 0$ followed by a series of secondary maxima. $H^d(x,\sigma,t)$ has a peculiar behavior having a maximum at $\sigma = 0$ for very small $-t$ and shows a diffraction pattern, while for relatively larger values of $-t$ it shows a minimum at $\sigma = 0$. The minima in $E(x,\sigma,t)$ occur at the same positions for both u- and d-quarks. In all cases, the position of the first minimum moves into smaller values of σ as $-t$ increases. The characteristics of $E(x,\sigma,t)$ for both u- and d-quarks are almost the same, whereas for $H(x,\sigma,t)$, the nature of u- and d-quark changes as $-t$ increases. In [21,22], similar diffraction patterns were observed for DVCS amplitudes with both $2 \to 2$ and $3 \to 1$ contributions, so we expect that the pattern will survive if higher Fock sectors are included in the model.

4 Transverse charge and magnetization densities

The two dimensional Fourier transform of the Dirac form factor gives the transverse charge density in the transverse plane for the unpolarized nucleons,

$$\rho_{\rm ch}(b) = \int \frac{{\rm d}^2 q_\perp}{(2\pi)^2} F_1(q^2) {\rm e}^{iq_\perp . b_\perp} = \int_0^\infty \frac{{\rm d}Q}{2\pi} Q J_0(Qb) F_1(Q^2), \tag{30}$$

where b represents the impact parameter and J_0 is the cylindrical Bessel function of order zero. We can write a similar formula for the charge density for flavor $\rho^q_{\rm fch}(b)$ with F_1 replaced by F_1^q. In a similar fashion, one defines the magneti-

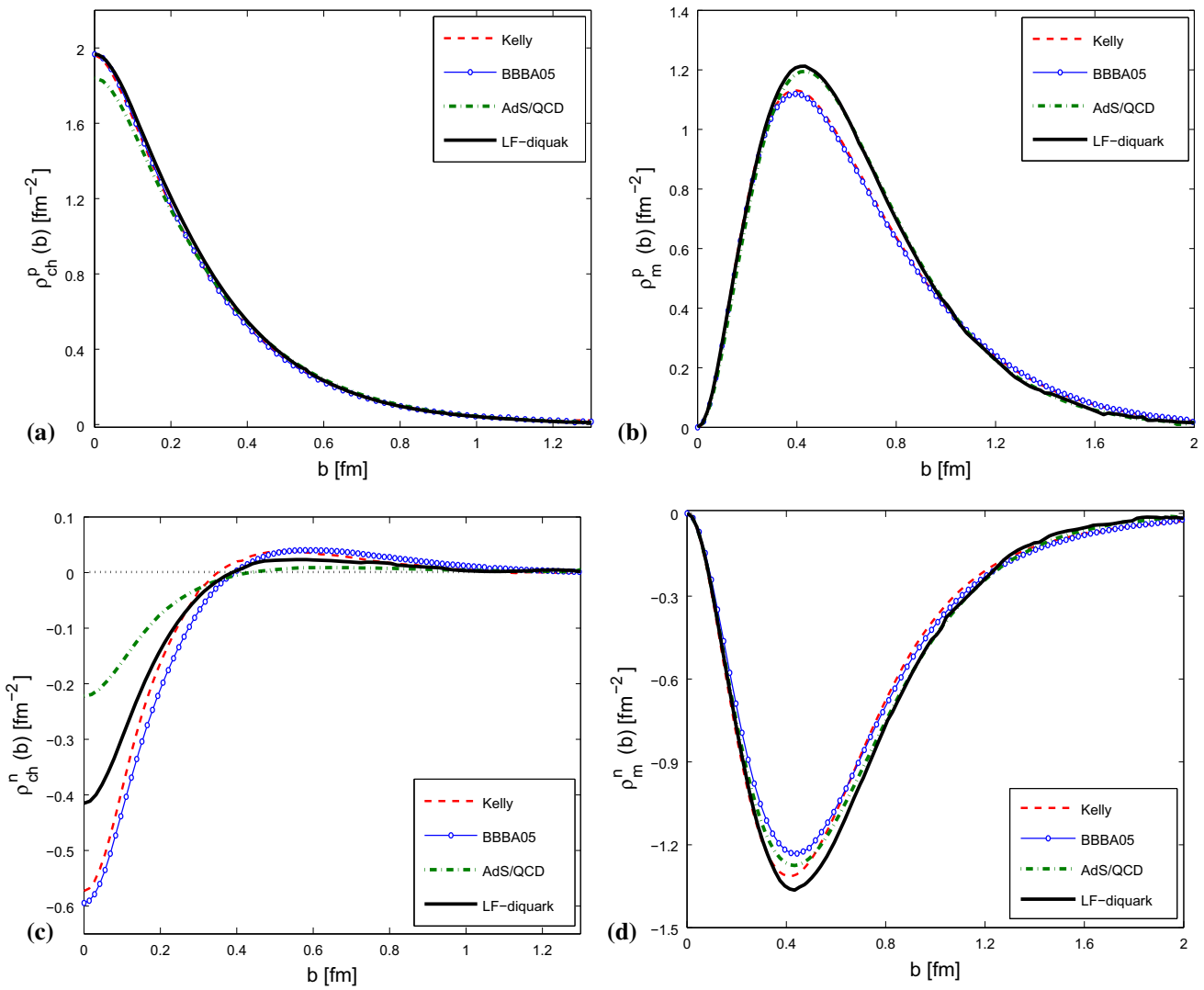

Fig. 13 Plots of transverse charge and anomalous magnetization densities for nucleon. **a** and **b** represent $\rho_{\rm ch}$ and $\rho_{\rm m}$ for the proton. **c** and **d** the same densities for the neutron. *Dashed lines* represent the parameterization of Kelly [27], and the *lines with circles* represent the parameterization of Bradford et al. [28], *dot-dashed lines* are for soft-wall model [29]. The *solid lines* represent the light-front scalar diquark model

zation density in the transverse plane by the Fourier transform of the Pauli form factor,

$$\widetilde{\rho}_{\rm M}(b) = \int \frac{{\rm d}^2 q_\perp}{(2\pi)^2} F_2(q^2) {\rm e}^{iq_\perp . b_\perp} = \int_0^\infty \frac{{\rm d}Q}{2\pi} Q J_0(Qb) F_2(Q^2), \quad (31)$$

whereas

$$\rho_{\rm m}(b) = -b\frac{\partial \widetilde{\rho}_{\rm M}(b)}{\partial b} = b\int_0^\infty \frac{{\rm d}Q}{2\pi} Q^2 J_1(Qb) F_2(Q^2), \quad (32)$$

has the interpretation of anomalous magnetization density [60]. Since these quantities are not directly measured in experiments, actual experimental data are not available. In Ref. [26], an estimation of the proton charge and magnetization densities has been done from experimental data of electromagnetic form factors. To get an insight into the contributions of the different flavors, we evaluate the charge and anomalous magnetization densities for the u- and d-quarks.

We can define the decompositions of the transverse charge and magnetization densities for nucleons in a similar way as electromagnetic form factors. The charge densities decompositions in terms of two flavors can be written as

$$\rho^p_{\rm ch} = e_u \rho^u_{\rm fch} + e_d \rho^d_{\rm fch}, \quad \rho^n_{\rm ch} = e_u \rho^d_{\rm fch} + e_d \rho^u_{\rm fch}, \quad (33)$$

where e_u and e_d are charge of the u- and d-quarks, respectively. Due to the charge and isospin symmetry the u- and d-quark densities in the proton are the same as the d and u densities in the neutron [29,63]. Under the charge and isospin symmetry, we can write

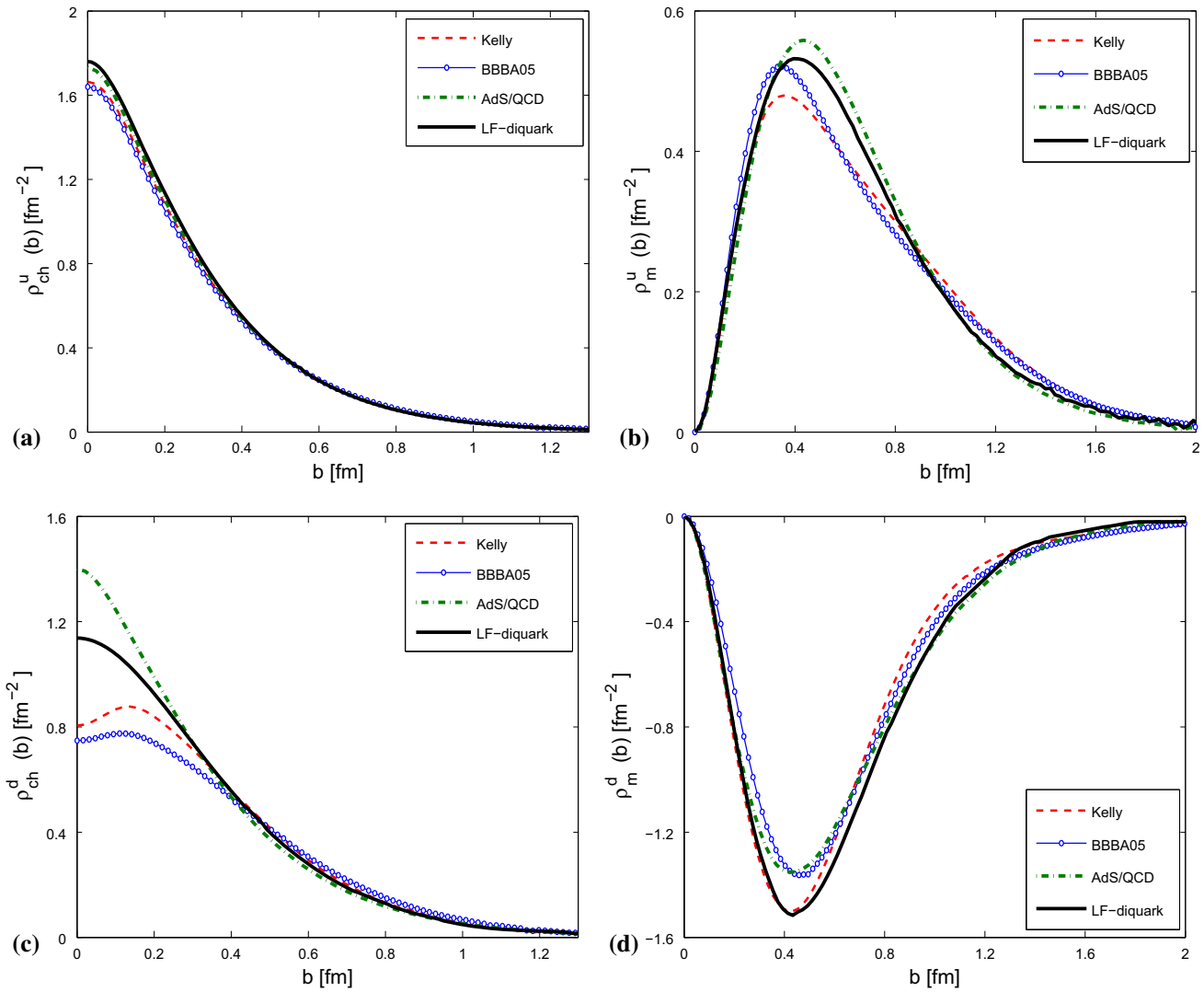

Fig. 14 Plots of transverse charge and anomalous magnetization densities for quark. **a** and **b** represent $\rho_{\rm ch}$ and $\rho_{\rm m}$ for the u-quark. **c** and **d** the same densities for the d-quark. *Dashed lines* represent the parameterization of Kelly [27], and the *lines with circles* represent the parameterization of Bradford et al. [28], *dot-dashed lines* are soft-wall model [29]. The *solid lines* represent the light-front scalar diquark model

$$\rho^u_{\rm ch}(b) = \rho^p_{\rm ch} + \frac{\rho^n_{\rm ch}}{2} = \frac{\rho^u_{\rm fch}}{2},$$
$$\rho^d_{\rm ch}(b) = \rho^p_{\rm ch} + 2\rho^n_{\rm ch} = \rho^d_{\rm fch}, \tag{34}$$

where $\rho^q_{\rm ch}(b)$ is the charge density of each quark and $\rho^q_{\rm fch}$ is the charge density for each flavor. We can similarly decompose $\rho_{\rm m}$ into magnetization densities for each flavor. The flavor contributions to the proton charge and magnetization densities are $e_{u/d}\rho^{u/d}_{\rm fch}$ and $e_{u/d}\rho^{u/d}_{\rm fm}$. Similarly for the neutron, the flavor contributions are $(e_{d/u}\,\rho^{u/d}_{\rm fch})$ and $(e_{d/u}\rho^{u/d}_{\rm fm})$.

In Fig. 13, we show the charge and anomalous magnetization densities for proton and neutron. The plots suggest that the light-front diquark model's results for the charge and magnetization density of proton and the magnetization density of neutron are in excellent agreement with the two different global parameterizations of Kelly [27] and Bradford et al. [28]. Though the diquark model is unable to reproduce the data for the neutron charge density at small b, still it is better than the AdS/QCD Model-I predictions presented in Ref. [29]. In Fig. 13c, one can notice a negatively charged core surrounded by a ring of positive charge density for the neutron. In Fig. 14a and b, we show the charge and anomalous magnetization densities for the u-quark. Similarly for the d-quark, the transverse densities are shown in Fig. 14c and d. The charge density for d-quark in the diquark model deviates at small b from the two global parameterizations of Kelly and Bradford but is in excellent agreement for the u-quark. Again, the diquark model provides a better result than the AdS/QCD Model-I results presented in Ref. [29]. The anomalous magnetization densities in both u- and d-quarks

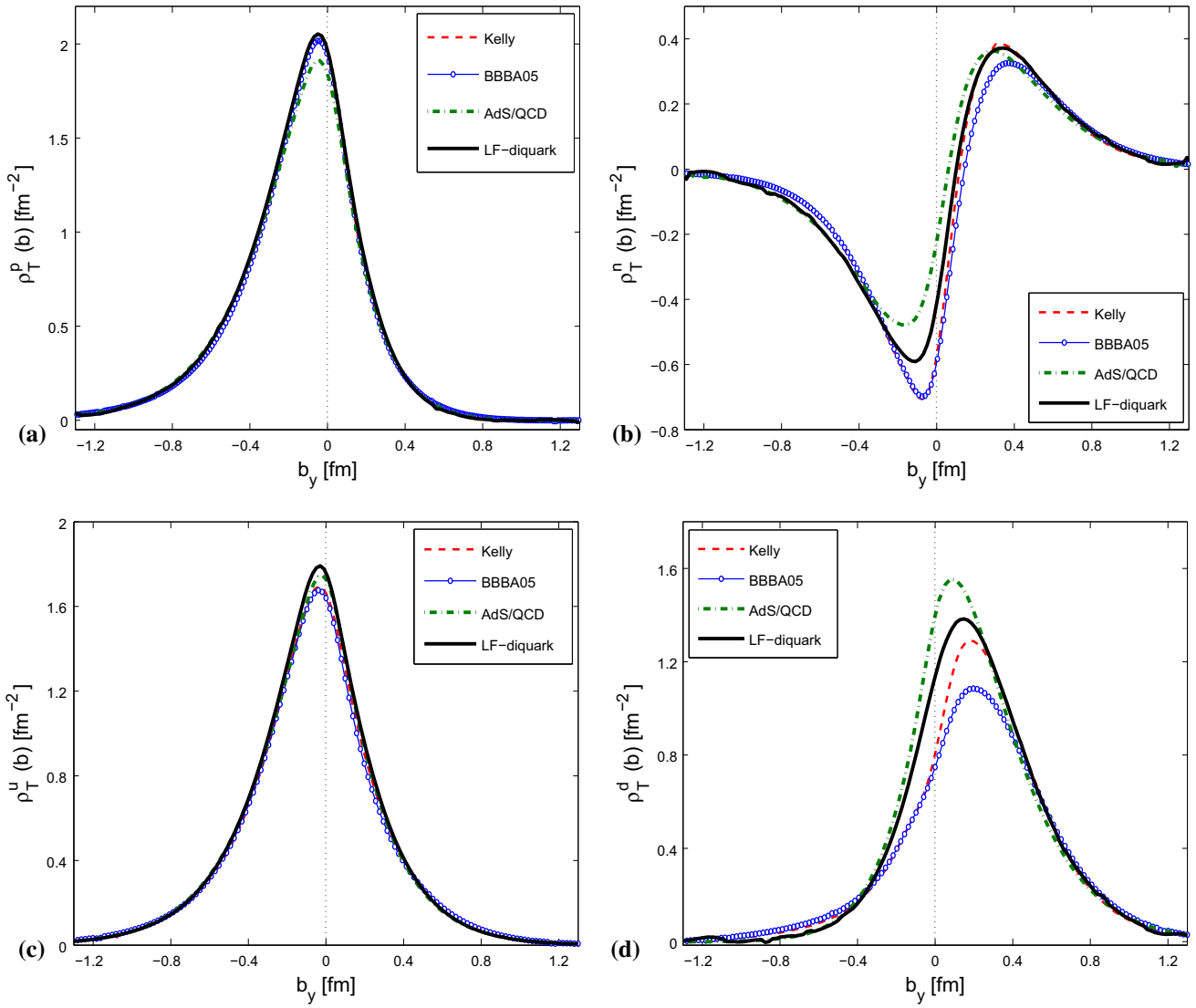

Fig. 15 The charge densities for the transversely polarized nucleons. **a** is for proton, **b** is for neutron. **c**, **d** up and down quark charge densities for the transversely polarized nucleon. The *dashed line* represents the parameterization of Kelly [27], and *line with circles* represents the parameterization of Bradford et al. [28], *dot-dashed line* is soft-wall Model-I in [29]. The *solid line* represents this work for light-front scalar diquark model

in the LF diquark model match very well the parameterizations.

For a transversely polarized nucleon, the charge density in the transverse plane is given by [61]

$$\rho_T(b) = \rho_{\rm ch} - \sin(\phi_b - \phi_s)\frac{1}{2Mb}\rho_{\rm m}, \tag{35}$$

where M is the mass of the nucleon and the transverse polarization of the nucleon is given by $S_\perp = (\cos\phi_s\hat{x} + \sin\phi_s\hat{y})$ and the transverse impact parameter $b_\perp = b(\cos\phi_b\hat{x} + \sin\phi_b\hat{y})$. Without loss of generality, the polarization of the nucleon is taken along the x-axis i.e., $\phi_s = 0$. The second term in Eq. (35) provides the deviation from circular symmetry of the unpolarized charge density [61]. The charge densities for the transversely polarized proton and neutron are shown in Fig. 15a and b. We show the u- and d-quark charge densities for the transversely polarized nucleon in Fig. 15c and d. Again, the densities in the LF diquark model are in good agreement with the global parameterizations. The comparison of charge densities for the transversely polarized and unpolarized proton is shown in Fig. 16a and b and similar plots for the neutron are shown in Fig. 16c and d. For the nucleons polarized along the x direction, the charge densities get shifted toward negative b_y direction for proton. The deviation is much larger for the neutron compared to the proton. Due to large anomalous magnetic moment which produces an induced electric dipole moment in y-direction, the distortion shows a dipolar pattern in the case of neutron [61]. The

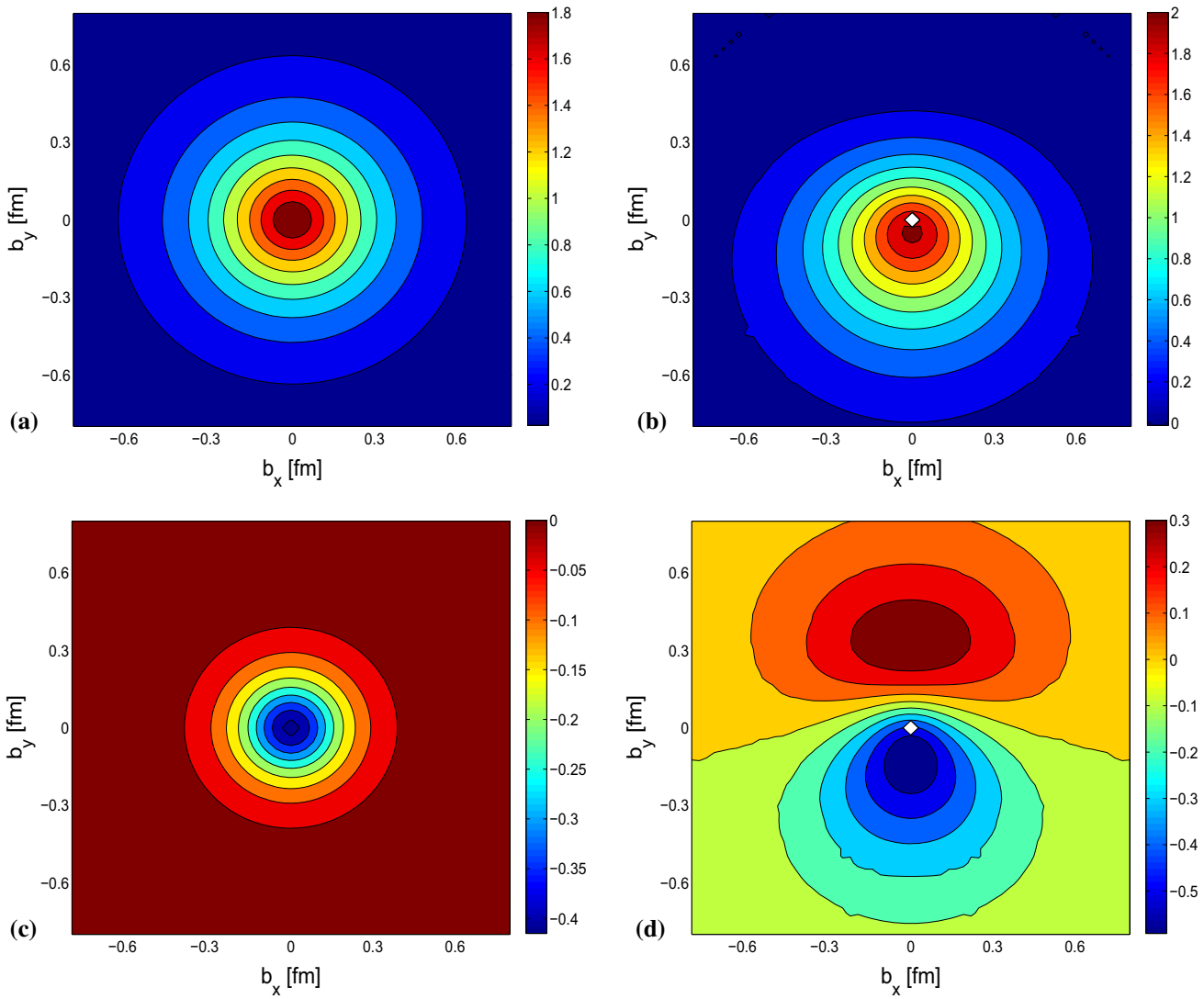

Fig. 16 The charge densities in the transverse plane, **a** is for a unpolarized proton, **b** is for a transversely polarized proton, **c** is for a unpolarized neutron, and **d** is for a transversely polarized neutron. Transverse polarization is along the x direction

behaviors are in agreement with the results reported in Refs. [60–62].

We compare the up quark charge densities for the transversely polarized and unpolarized nucleon in Fig. 17a and b and similar plots for the d-quark are shown in Fig. 17c and d. The deviation or distortion from the symmetric unpolarized density is more for down quark than the up quark. For the nucleons polarized in x direction, the charge density shifts toward positive b_y direction for the d-quark but in opposite direction for the u-quark.

5 Summary and conclusions

The parameters in a light-front quark–diquark model of the nucleons [1] are found to be inconsistent with the experimental data. We have re-evaluated the parameters in this model for the AdS/QCD scale parameter $\kappa = 0.4066$ GeV, which was previously obtained by fitting the nucleon form factors in soft-wall AdS/QCD [14,35]. The new parameters reproduce the experimental data for the nucleon form factor quite well for a wide range of Q^2 values. We have compared our results with AdS/QCD soft-wall model. Then we have evaluated the GPDs for u- and d-quark in proton for both zero and nonzero skewness in the light-front quark–diquark model. We observed that all the GPDs in the momentum space as well as in the transverse impact parameter space are more or less in agreement with the results of AdS/QCD. We have calculated the GPDs for nonzero skewness in the DGLAP region (i.e., for $x > \zeta$). The peaks of the distributions move to higher values of x for fixed ζ with increasing $-t$. In the model, the behaviors of the GPD H in impact parameter space for u-

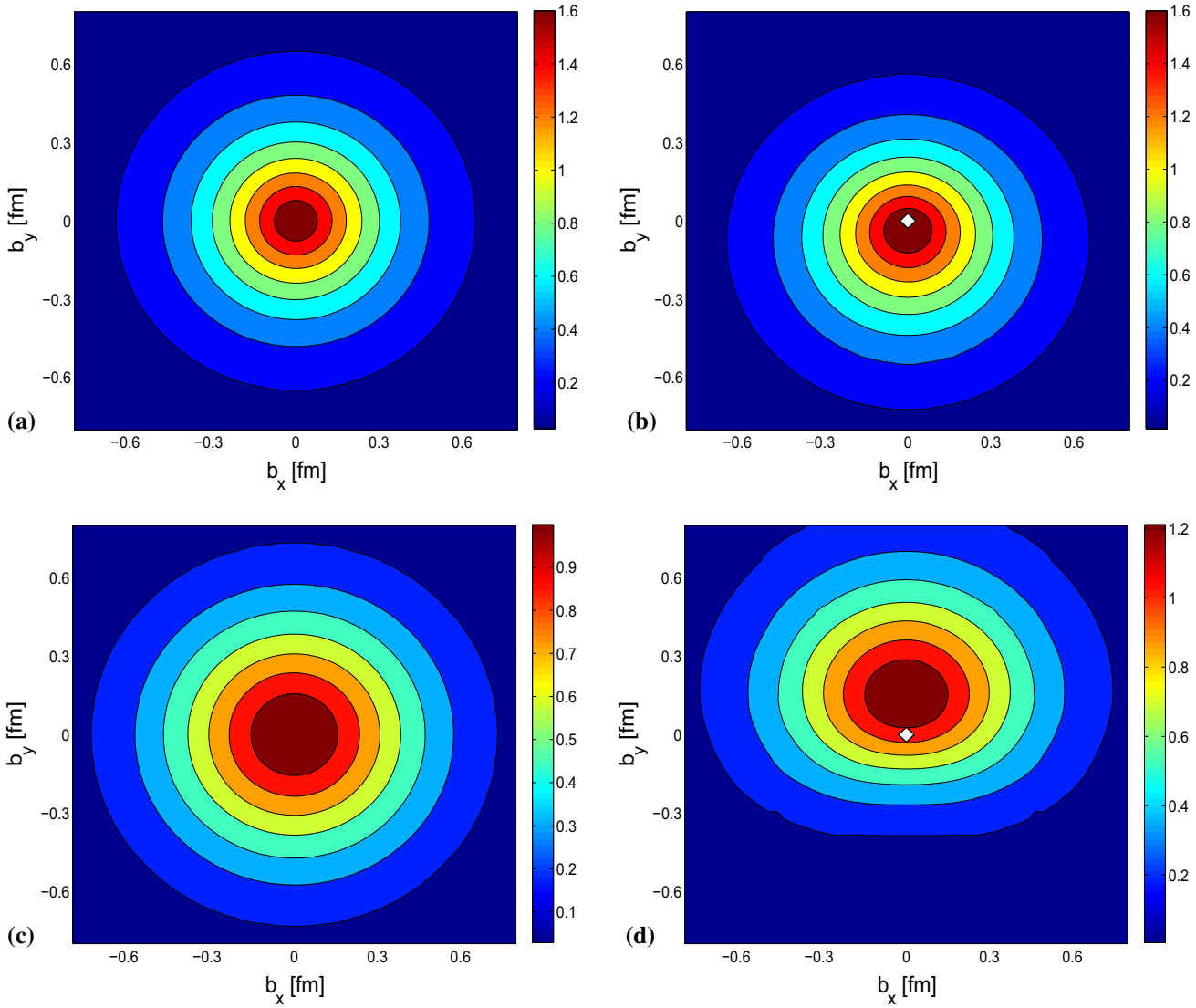

Fig. 17 The charge densities in the transverse plane, **a** is for u-quark in a unpolarized nucleon, **b** is for u-quark in a transversely polarized nucleon and **c** is for d-quark in a unpolarized nucleon, **d** is for d-quark in a transversely polarized nucleon. Polarization is along x-direction

and d-quarks are quite different when plotted in both x and b. The difference in the behaviors of $E(x, \zeta, t)$ for u- and d-quarks are clearly observed when plotted against x. For nonzero skewness, we have also shown the GPDs in longitudinal impact parameter space σ. We found that both the GPDs H and E for u- and d-quarks in σ space show diffraction patterns. Similar diffraction patterns also have been observed in some other models. In the case of $E(x, \sigma, t)$, the qualitative nature of the diffraction pattern is the same for both u- and d-quarks. For $H^d(x, \sigma, t)$, the diffraction pattern is observed only for small $-t$ values; as $-t$ increases, a dip appears at the center (at $\sigma = 0$).

Finally, we have presented the transverse charge and magnetization densities for nucleon and also for individual quarks. The results are consistent with two phenomenological parameterizations [27,28]. The unpolarized densities are axially symmetric, whereas the charge densities get distorted for a transversely polarized nucleon. The charge density is shifted along the y direction if the nucleon is polarized along the x direction. The charge density for a transversely polarized neutron shows a dipole pattern. The shift of charge density of u-quark for a transversely polarized nucleon from the symmetric unpolarized density is smaller than the d-quark and in an opposite direction.

Funded by SCOAP[3].

Appendix A: Comparison of GPDs in the quark–diquark model with a double distribution (DD) model

The GPDs for $\zeta = 0$ admit a density interpretation when one takes the Fourier transform to the impact parameter space but in experiments, ζ is always nonzero. In the recent past, there has been a lot of work to model GPDs with nonzero skewness by modeling relevant DDs [64,65]. In this section, we compare our results for nonzero skewness with the GPDs modeled from the Double Distributions (DD) [66–68].

The GPDs have an integral representation in terms of the double distributions $f(\beta, \alpha, t)$. For the valence quarks, the GPDs can be written as

$$F_v^q(x,\zeta,t) = \int_0^1 \mathrm{d}\beta \int_{\beta-1}^{1-\beta} \mathrm{d}\alpha\ \delta(x-\beta-\zeta\alpha)\ f_v^q(\beta,\alpha,t), \tag{A.1}$$

where $F_v^q = H_v^q, E_v^q$. Here, we use the factorized DD ansatz for the GPDs as suggested by Musatov and Radyushkin [69]

$$f_v^q(\beta,\alpha,t) = F_v^q(\beta,0,t)h(\beta,\alpha), \tag{A.2}$$

where the weight function $h(\beta,\alpha)$ generates the skewness dependence of the GPDs and satisfies the normalization condition

$$\int_{-1+|\beta|}^{1-|\beta|} h(\beta,\alpha)\mathrm{d}\alpha = 1. \tag{A.3}$$

The general form of the profile function is given by [69]

$$h^{(N)}(\beta,\alpha) = \frac{\Gamma(2N+2)}{2^{2N+1}\Gamma^2(N+1)} \frac{[(1-|\beta|)^2-\alpha^2]^N}{(1-|\beta|)^{2N+1}}, \tag{A.4}$$

where the parameter N governs the width of the function. We use the $N = 2$ profile function. A similar profile function for $N = 2$ has been used in many phenomenological models of

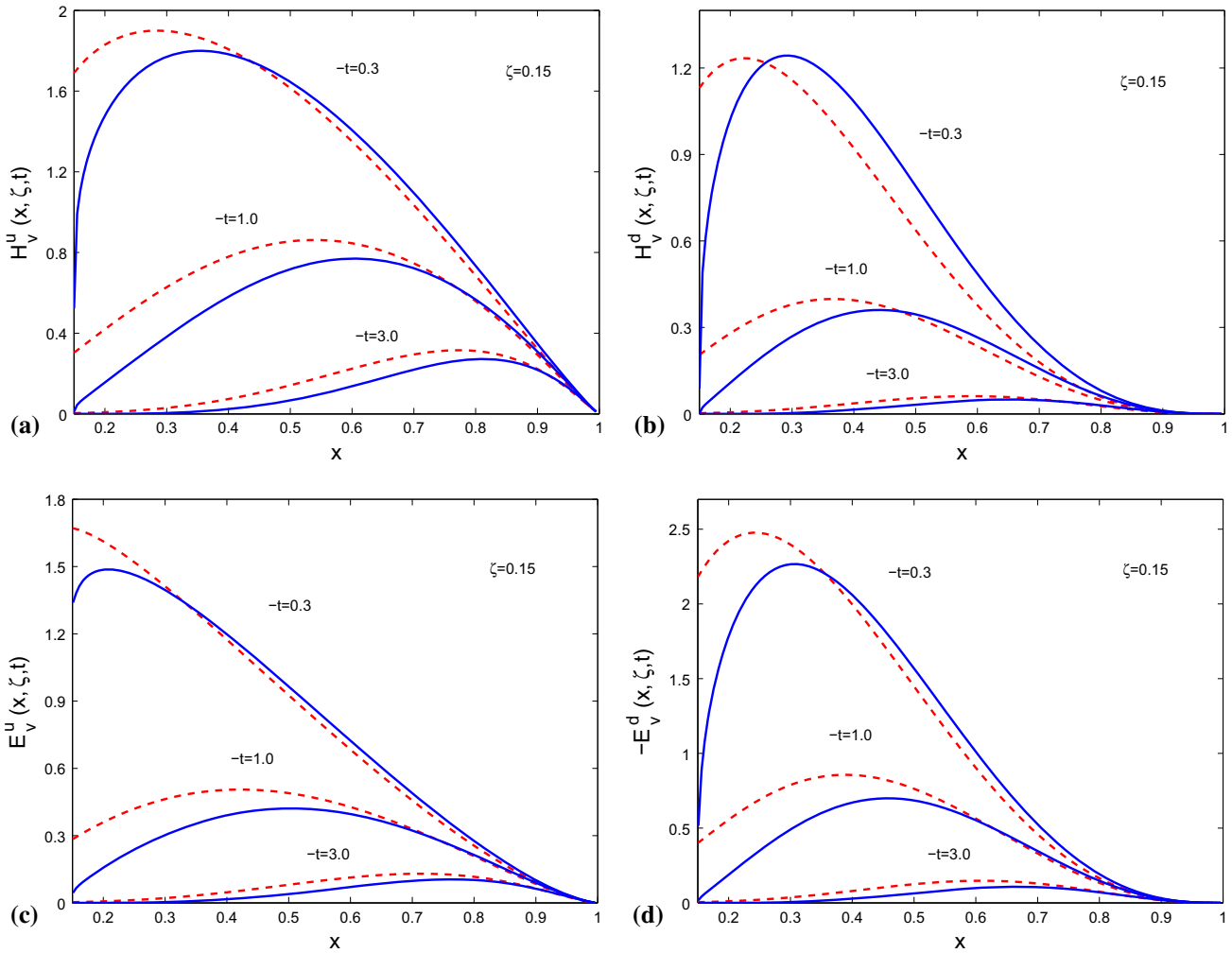

Fig. 18 Comparison of GPDs in the quark-diquark model with the DD model for a fixed value of $\zeta = 0.15$ and three different values of $-t = 0.3, 1.0, \&3.0\ \mathrm{GeV}^2$. *Red dashed lines* represent the results in the DD model

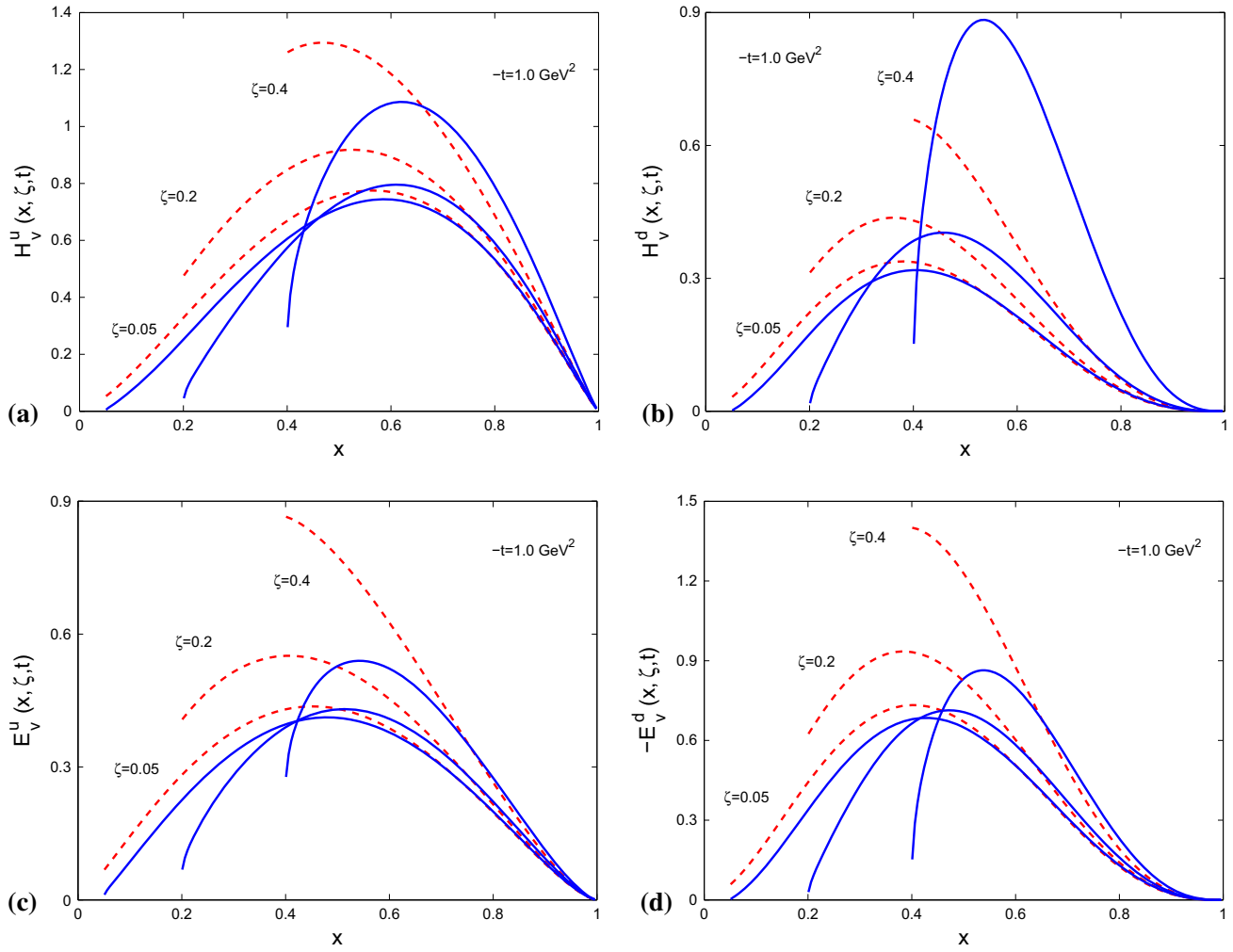

Fig. 19 Comparison of GPDs in the quark-diquark model with the DD model for a fixed value of $-t = 1.0$ GeV^2 and three different values of $\zeta = 0.05, 0.2, \&0.4$. *Red dashed lines* represent the results in the DD model

DVCS and exclusive meson production [4–6,70–72]. Inserting Eq. (A.2) in Eq. (A.1), with the help of the delta-function one can perform the integral over α and obtains

$$F_v^q(x,\zeta,t) = \frac{3}{4\zeta^3}\int_{\beta_{\min}}^{\beta_{\max}} \frac{\mathrm{d}\beta}{1-\beta}\, F_v^q(\beta,0,t) \times \Big(1+\zeta-\frac{1-x}{1-\beta}\Big)\Big(\frac{1-x}{1-\beta}-1+\zeta\Big), \tag{A.5}$$

for $x > \zeta$, the integration boundaries are

$$\begin{aligned} \beta_{\min} &= x - \frac{\zeta}{1-\zeta}(1-x), \\ \beta_{\max} &= x + \frac{\zeta}{1-\zeta}(1-x). \end{aligned} \tag{A.6}$$

In Figs. 18 and 19, we show the skewness dependent GPDs calculated using double distribution parameterization and compare with the results directly calculated in the quark–diquark model. Figure 18 suggests that for small ζ and large $-t$, the results of double distribution are more or less in agreement with the diquark model results, while Fig. 19 shows that at moderate or high values of skewness ζ, only at higher x the two models agree but otherwise the agreement is lost.

References

1. T. Gutsche, V.E. Lyubovitskij, I. Schmidt, A. Vega, Phys. Rev. D **89**, 054033 (2014)
2. G.F. de Teramond, H.G. Dosch, S.J. Brodsky, Phys. Rev. D **91**(4), 045040 (2015)
3. J.R. Forshaw, R. Sandapen, Phys. Rev. Lett. **109**, 081601 (2012)
4. M. Diehl, Phys. Rep. **388**, 41 (2003)
5. A.V. Belitsky, A.V. Radyushkin, Phys. Rep. **418**, 1 (2005)
6. K. Goeke, M.V. Polyakov, M. Vanderhaeghen, Prog. Part. Nucl. Phys. **47**, 401 (2001)
7. X. Ji, Phys. Rev. Lett. **78**, 610 (1997)
8. M. Burkardt, Int. J. Mod. Phys. A **18**, 173 (2003)
9. A. Ferrero (COMPASS Collaboration), J. Phys. Conf. **295**, 012039 (2011)
10. A. Adolph et al. (COMPASS), Phys. Lett. B **731**, 19 (2014)

11. A. Airapetian et al. (HERMES Collaboration), Nucl. Phys. B **842**, 265 (2011)
12. A. Airapetian et al. (HERMES Collaboration), Phys. Lett. B **704**, 15 (2011)
13. C.M. Camachao et al. (JLAB HALL A Collaboration), Phys. Rev. Lett. **97**, 262002 (2006)
14. D. Chakrabarti, C. Mondal, Phys. Rev. D **88**, 073006 (2013)
15. S.J. Brodsky, G.F. de Téramond, Phys. Lett. B **582**, 211 (2004)
16. S.J. Brodsky, G.F. de Téramond, Phys. Rev. Lett. **94**, 201601 (2005)
17. S.J. Brodsky, G.F. de Téramond, Phys. Rev. Lett. **96**, 201601 (2006)
18. S.J. Brodsky, G.F. de Téramond, Phys. Rev. D **77**, 056007 (2006)
19. S.J. Brodsky, G.F. de Téramond, Phys. Rev. Lett. **102**, 081601 (2009)
20. Z. Abidin, C.E. Carlson, Phys. Rev. D **79**, 115003 (2009)
21. S.J. Brodsky, D. Chakrabarti, A. Harindranath, A. Mukherjee, J.P. Vary, Phys. Lett. B **641**, 440 (2006)
22. S.J. Brodsky, D. Chakrabarti, A. Harindranath, A. Mukherjee, J.P. Vary, Phys. Rev. D **75**, 014002 (2007)
23. D. Chakrabarti, R. Manohar, A. Mukherjee, Phys. Rev. D **79**, 034006 (2009)
24. R. Manohar, A. Mukherjee, D. Chakrabarti, Phys. Rev. D **83**, 014004 (2011)
25. G.A. Miller, Phys. Rev. C **80**, 045210 (2009)
26. S. Venkat, J. Arrington, G.A. Miller, X. Zhan, Phys. Rev. C **83**, 015203 (2011)
27. J.J. Kelly, Phys. Rev. C **70**, 068202 (2004)
28. R. Bradford, A. Bodek, H. Budd, J. Arrington, Nucl. Phys. Proc. Suppl. **159**, 127 (2006)
29. D. Chakrabarti, C. Mondal, Eur. Phys. J. C **74**, 2962 (2014)
30. S.J. Brodsky, S.D. Drell, Phys. Rev. D **22**, 2236 (1980)
31. S.J. Brodsky, D.S. Hwang, Nucl. Phys. B **543**, 239 (1999)
32. S.J. Brodsky, D.S. Hwang, B.-Q. Ma, I. Schmidt, Nucl. Phys. B **593**, 311 (2001)
33. S.J. Brodsky, M. Diehl, D.S. Hwang, Nucl. Phys. B **596**, 99 (2001)
34. S.J. Brodsky, G.F. de Téramond, arXiv:1203.4025 [hep-ph]
35. D. Chakrabarti, C. Mondal, Eur. Phys. J. C **73**, 2671 (2013)
36. J. Beringer et al. (Particle data Group), Phys. Rev. D. **86**, 010001 (2012)
37. I.A. Qattan, J. Arrington, Phys. Rev. C **86**, 065210 (2012)
38. P. Schweitzer, S. Boffi, M. Radici, Phys. Rev. D. **66**, 114004 (2002)
39. P. Schweitzer, M. Colli, S. Boffi, Phys. Rev. D **67**, 114022 (2003)
40. G.D. Cates, C.W. de Jager, S. Riodian, B. Wojtsekhowski, Phys. Rev. Lett. **106**, 252003 (2011)
41. M. Diehl, P. Kroll, Eur. Phys. J. C **73**, 2397 (2013)
42. O. Gayou et al., Phys. Rev. C **64**, 038202 (2001)
43. O. Gayou et al., Phys. Rev. Lett. **88**, 092301 (2002)
44. J. Arrington, W. Melnitchouk, J.A. Tjon, Phys. Rev. C **76**, 035205 (2007)
45. V. Punjabi et al., Phys. Rev. C **71**, 055202 (2005)
46. A. Puckett et al., Phys. Rev. Lett. **104**, 242301 (2010)
47. C. Herberg et al., Eur. Phys. J. A **5**, 131 (1999)
48. D.I. Glazier et al., Eur. Phys. J. A **24**, 101 (2005)
49. B. Plaster et al., Phys. Rev. C **73**, 025205 (2006)
50. J. Bermuth et al., Phys. Lett. B **564**, 199 (2003)
51. S. Riordan et al., Phys. Rev. Lett. **105**, 262302 (2010)
52. G. Warren et al., Phys. Rev. Lett. **92**, 042301 (2004)
53. I. Passchier et al., Phys. Rev. Lett. **82**, 4988 (1999)
54. H. Zhu et al., Phys. Rev. lett. **87**, 081801 (2001)
55. E.J. Geis, Ph.D. thesis, UMI-32-58089
56. M. Burkardt, Phys. Rev. D **62**, 071503 (2000) (erratum- ibid, Phys. Rev. D 66, 119903, 2002)
57. J.P. Ralston, B. Pire, Phys. Rev. D **66**, 111501 (2002)
58. M. Diehl, T. Feldman, R. Jacob, P. Kroll, Eur. Phys. J. C **39**, 1 (2005)
59. D. Chakrabarti, R. Manohar, A. Mukherjee, Phys. Lett. B **682**, 428 (2010)
60. G.A. Miler, Annu. Rev. Nucl. Part. Sci. **60**, 1 (2010)
61. C.E. Carlson, M. Vanderhaeghen, Phys. Rev. Lett. **100**, 032004 (2008)
62. A. Silva, D. Urbano, H. Kim, arXiv:1305.6373 [hep-ph]
63. G.A. Miller, Phys. Rev. Lett. **99**, 112001 (2007)
64. A.V. Radyushkin, Phys. Rev. D **83**, 076006 (2011)
65. A.V. Radyushkin, Phys. Rev. D **87**, 096017 (2013)
66. D. Müller, D. Robaschik, B. Geyer, F.-M. Dittes, J. Hořejši, Fortsch. Phys. **42**, 101 (1994)
67. X.D. Ji, Phys. Rev. D **55**, 7114 (1997)
68. A.V. Radyushkin, Phys. Lett. B **449**, 81 (1999)
69. I.V. Musatov, A.V. Radyushkin, Phys. Rev. D **61**, 074027 (2000)
70. S.V. Goloskokov, P. Kroll, Eur. Phys. J. C **53**, 367 (2008)
71. S.V. Goloskokov, P. Kroll, Eur. Phys. J. C **59**, 809 (2009)
72. M. Diehl, W. Kugler, A. Schäfer, C. Weiss, Phys. Rev. D **72**, 034034 (2005)